Aalto University

Balboa, I.; Rose, E.; Matthews, G. F.; Croft, D.; Stamp, M. F.; Silburn, S. A.; Williams, J. C.; Hepple, D.; Huber, A.; Whetham, S.; Iglesias, D.; Kinna, D. J.; Beldishevski, M.; Figueiredo, J.; Perez Von Thun, C.; Balshaw, N.; Horton, L. D.; Lobel, R. C.; Pearson, I. J.; Pepperell, K. W.; Fishpool, G.; Lane, B.; Zastrow, K. D.; Arnoux, G.; Bodnar, G.; Carman, P.; Carvalho, P.; Conway, N. J.; Huber, V.; Karhunen, J.; Kocsis, G.; Manzanares, A.; Puglia, P.; Ruíz de Galarreta, C.; Marren, C.; Naish, J.; Thompson, V. K.; JET Contributors

Remote infrared view of JET divertor compatible with D-T operations

Remote infrared view of JET divertor compatible with D-T operations

View the article online for updates and enhancements.

Remote infrared view of JET divertor compatible with D-T operations

I Balboa[1,*] , E Rose[1], G F Matthews[1], D Croft[1], M F Stamp[1], S A Silburn[1] , J C Williams[1],
D Hepple[1], A Huber[2] , S Whetham[1], D Iglesias[1,10], D J Kinna[1], M Beldishevski[1],
J Figueiredo[3,4], C Perez Von Thun[2,11] , N Balshaw[1], L D Horton[5,6], R C Lobel[1],
I J Pearson[1], K W Pepperell[1], G Fishpool[1], B Lane[1], K-D Zastrow[1], G Arnoux[1], G Bodnar[7],
P Carman[1], P Carvalho[1,3], N J Conway[1], V Huber[2], J Karhunen[8,12] , G Kocsis[7],
A Manzanares[9], P Puglia[1,6], C Ruíz de Galarreta[9], C Marren[1], R Otín[1], J Naish[1],
V K Thompson[1] and the JET Contributors[13]

[1] United Kingdom Atomic Energy Authority, Culham Science Centre, Abingdon, Oxon OX14 3DB, United Kingdom
[2] Forschungszentrum Jülich GmbH, Institut für Energie und Klimaforschung, Plasmaphysik, 52425 Jülich, Germany
[3] Instituto de Plasma e Fusão Nuclear, Instituto Superior Técnico, Universidad de Lisboa, 1049-001 Lisboa, Portugal
[4] EUROfusion Programme Management Unit, Boltzmannstr. 2, 85748 Garching, Germany
[5] EUROfusion Programme Management Unit, Culham Science Centre, Culham OX14 3DB, United Kingdom
[6] Ecole Polytechnique Fédérale de Lausanne (EFPL), Swiss Plasma Center (SPC), CH-1015 Lausanne, Switzerland
[7] Centre for Energy Research, POB 49, H-1525 Budapest, Hungary
[8] Department of Applied Physics, Aalto University, PO Box 11000, 00076 Aalto, Finland
[9] Laboratorio Nacional de Fusión, CIEMAT, Madrid, Spain

E-mail: itziar.balboa@ukaea.uk

CrossMark

Abstract

A remote viewing system located outside the biological shield wall to image the divertor region in JET is presented here. This paper focuses on the optical and mechanical designs of the installation of a line of sight which is capable of imaging the divertor over an optical distance of approximately 31 m. In addition, it includes the experience obtained during operations and it demonstrates its successful performance. This line of sight was the second viewing system used during the D-T campaign and it follows from the paper dedicated to the remote wide angle view line of sight which is also compatible with D-T operations and includes common elements to the construction of the two lines of sight. The main novel feature is the design in house of two glass reinforced plastic kinematic mounts standing vertically to each accommodate a mirror of 500 mm in diameter.

---

[10] Currently at ITER organization, Route de Vinon-sur-Verdon, CS90 046, 13067 Saint Paul Lez Durance Cedex, France.
[11] Currently at Institute of Plasma Physics and Laser Microfusion, Hery 23, 01-497 Warsaw, Poland.
[12] Currently at VTT Technical Research Centre of Finland, PO Box 1000, 02044 VTT, Finland.
[13] See the author list of 'Overview of JET results for optimising ITER operation' by J. Mailloux *et al.* 2022 *Nuclear Fusion* **62** 042026.
[*] Author to whom any correspondence should be addressed.

1. Introduction

The second deuterium-tritium (D-T) experimental campaign in JET during the second half of 2021, marked the achievement of an essential milestone to demonstrate the potential of magnetic confinement fusion for tokamaks (see [1]). Furthermore, the scientific results obtained prior (see [2]) and during the D-T experimental campaign (at the time of preparing this paper, a new set of publications related to the scientific exploitation of the D-T campaign are in the process of being finalised in the next few months by the respective scientific teams and they will be published in the Special Issue in Nuclear Fusion) are also critical for the design and operation of future machines such as ITER.

JET diagnostics have played a vital role in the achievement of this milestone. However, it was necessary to ensure, ahead of the D-T experimental campaign, that key diagnostics were going to be compatible with D-T operations due to significantly higher radiation levels in the machine hall (see [3]). To this effect, a program of diagnostic enhancements, known as 'Diagnostic Enhancements for D-T Operations' (WPJET4), was launched; it was funded by EUROfusion and JET Operating Contract (JOC) (see [4, 5]).

Among this program of diagnostic enhancements, a project for the re-design of multiple viewing systems to be moved outside the machine hall (i.e., Torus Hall) was included. This project was entitled 'Cameras compatible with D-T operations'. The scope of this project was the relocation of selected camera diagnostics from the inside of the Torus Hall to the outside the biological shield wall since the neutron flux during the D-T reaction would have impacted the electronics of the viewing systems causing some of them to fail after just one D-T pulse.

Two separate lines of sight have been designed, installed and commissioned ahead of the D-T campaign. Once the D-T campaign started, these two lines of sight connected a set of cameras from the outside of the biological shield wall to the plasma and, most importantly, they were the only imaging capabilities during the D-T campaign in JET since all the other existing camera systems prior to the beginning of the D-T campaign had been removed.

These two lines of sight are known as 'Wide Angle View' (WAV) and 'Divertor Infrared View' (DIR). As mentioned earlier, each line of sight (LOS) is capable of imaging the plasma facing components from outside the biological shield wall into a number of camera systems associated to each of the lines of sight. This paper, however, is covering only the design, installation and operational experience phases of the DIR line of sight. There is a companion paper which is dedicated to the WAV line of sight regarding its design and operation (see [6]) which includes some aspects of the design that are common to both lines of sight.

It was essential to retain a view of the JET divertor because of the crucial role that the infrared imaging diagnostics play in the protection of the horizontal divertor tiles and the understanding of the thermal loads and plasma interactions in the divertor region.

Direct examples of applications of thermal imaging for the operation and scientific exploitation of experiments in JET can be found in [7, 8]. Although some of the design presented in this manuscript is based on the same concept as WAV, due to the technical requirements for the DIR LOS, there are still significant differences to merit the writing of a second paper dedicated exclusively to the DIR LOS. This paper therefore covers the optical and mechanical designs of the entire DIR system. The most relevant novel feature is the design of a kinematic mirror mount made of glass reinforced plastic (GRP) for an optical mirror of 500 mm diameter standing vertically. The DIR LOS extends beyond the Torus Hall into labs in the adjacent building which are shared with the WAV system. The WAV paper will be referenced for components where there are shared or similar engineering solutions.

The outline of this paper is as follows: it starts with a description of the target field of view. It then follows with section 3 dedicated to the entire DIR LOS to provide the reader with an overview of the entire system as to how the target field of view has been achieved. The viewing systems included in the LOS and their specifications are then listed in section 4, followed by descriptions of the optical (see section 5) and mechanical designs. The mechanical design section is split between those structures inside the Torus Hall and those outside, corresponding to sections 6 and 7 respectively. In addition, there will be a different section for the penetrations in the biological shield wall, which is the optical bridge between the components inside the Torus Hall and outside (see section 8). The mounting of the viewing systems is presented in section 9. Finally, the operational performance of the camera system during the D-T campaign will be described in section 10.

2. Field of view

The target for the system was to reproduce the field of view and performance of a camera diagnostic which was located on top of the upper vertical port prior to the construction of the DIR LOS. Two pictures of the divertor region inside the tokamak are provided below (see figure 1). The picture on the left depicts the side view of the divertor where the orange boxed area shows tiles in the target field of view. The tile structure shown on the side view repeats itself all around the tokamak. On the other hand, the picture on the right is the CAD model of a top view looking down into the divertor where the orange boxed area represents the target field of view.

As seen in figure 1, the target field of view includes the main horizontal tile, denoted as Tile 5, and its four stacks referred to as 'A', 'B', 'C', and 'D'. Each stack is formed of 24 individual elements. Each element is a tungsten blade called a 'lamella'
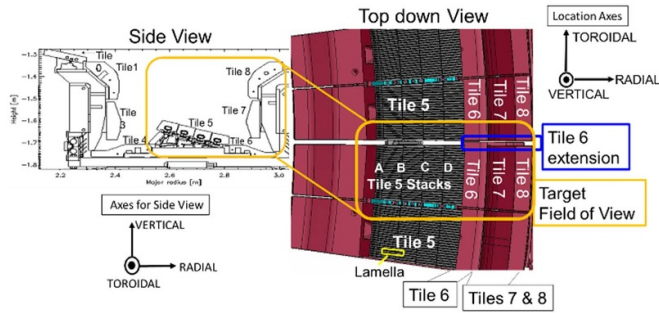
Figure 1. Left: Side view of divertor region with an orange boxed area representing the target field of view. Right: Top view of divertor region from CAD model with orange boxed area to show target field of view.

Figure 2. Schematic of the DIR line of sight.

(see [9]). In addition, it covers the horizontal Tile 6 and Tile 6 extension between Tiles 7 and 8 as well as these two tiles. Tile 7 and Tile 8 are vertical tiles. It is not possible to distinguish between the vertical tiles 7 and 8 because Tile 8 nearly completely obscures the view of Tile 7 when looking from above. In addition, Tiles 7 and 8 obscure the section of Tile 6 which is underneath. Tile 6 was extended toroidally in between the gap of Tiles 7 and 8 for the modules in the location of this field of view to allow the IR cameras to view the otherwise obscured section. Tile 6 is used frequently in plasma scenarios as the horizontal target for the outer strike point because it improves confinement (see [10]). Thus, it is important to use imaging diagnostics such as camera systems operating in the infrared in order to monitor and analyse the thermal loads as part of the plasma scenario development (see [11]). The extension of the Tile 6 was carried out only in Octant 5 and took place in 2014 during a JET shutdown. The difference in colour (which is only for illustrative purposes) between the Tile 5 and the rest of the other tiles is due to the tile material, which for Tile 5 is bulk tungsten and for the rest of the divertor tiles is tungsten coated (see [12]).

3. Line of sight

The DIR line of sight was built to enable the imaging of the divertor region from outside the Torus Hall. The main requirements for the design of the line of sight were first to use the octant where the Tile 6 extension was located and secondly to identify the shortest and simplest route which had also to include an adjacent building to house the viewing systems. The LOS has been depicted in figure 2. This is a view through one of the main upper vertical ports in the machine. This vertical port includes a double window which is a requirement to reduce the risk of a tritium leak from the tokamak into the Torus Hall. A bespoke mirror based optical relay was designed and built for the LOS which consists of several mirror mounting assemblies located inside and outside the Torus Hall. The name convention of the mirror assemblies follows the sequence of reflections from each mirror. There are three optical assemblies inside the Torus Hall which are known as 'L1-M1-M2', 'M3' and 'M4'. The LOS traverses through the
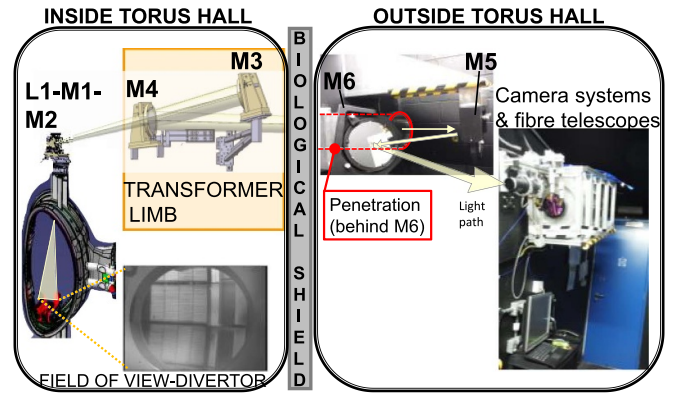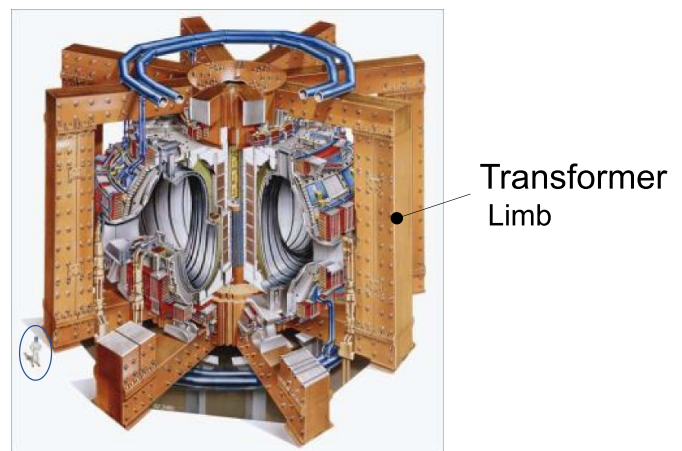

Figure 3. JET tokamak picture showing the transformer limbs. The size of the JET tokamak has been compared with to a person's size (see [13]).

biological shield into the adjacent building (known as 'J1F') to the west side of the Torus Hall. The total optical length is 31 m.

A picture of the JET tokamak is included in figure 3 in order to provide some context of the JET tokamak and the transformer limbs located around each of its eight octants. As depicted in figure 3, the transformer structure has been integrated forming a 'limb' into each of the octants (see [13]). For the case of the DIR line of sight, the mirror assemblies denoted as 'M3' and 'M4' have been fixed to the transformer limb identified as '5/6' which is the opposite limb to the one used to fix the mirror assemblies for the wide angle view line of sight (see [6]).

Outside the Torus Hall, three labs were constructed along the vertical direction, although the DIR system only uses two of these labs. In addition, there are two mirror assemblies known as 'M5' and 'M6'. Figure 2 shows the 'L1-M1-M2' assembly installed on top of the upper vertical port of the machine whereas 'M3' and 'M4' are attached to the transformer limb. A photo of the field of view showing the divertor region is also included in figure 2. At the other side of the biological shield wall, there are 'M5' and 'M6' assemblies. The penetration through the biological shield wall has

been depicted on the right-hand side of figure 2 with a red coloured dashed line because it is located just behind the M6 mirror. In addition, there is a second photo from inside one of the labs where the viewing systems are located.

4. System specifications

The list of viewing systems is presented in table 1. There are two applications: the protection of the divertor tiles and the production of temperatures and heat fluxes in support of the experimental campaign. The selection of the systems listed in this section was driven by the requirement of reproducing identical or close performance to the imaging diagnostics located inside the Torus Hall. The main operating wavelength range is the near infrared which is used by the protection camera (KLDT-P5TB) and four fibre telescopes used by two pyrometers and two spectrometers. The exception is the scientific camera (KLDT-E5TA) which is used for production of temperature and heat fluxes and operates in the middle wavelength infrared range (MWIR).

The specifications of the DIR camera systems are listed in table 2. A distinction has been made between the MWIR scientific camera (KLDT-E5TA) installed until 2019 and the second unit which was installed after 2019 to replace the first one after it failed. They both have the same sensor type: InSb focal plane arrays cooled to ∼77 K using a Stirling cooler integrated with complementary metal-oxide-semiconductor readout circuitry. The advantage of this type of sensor is that it is possible to select different regions of interest (ROI) which enables increasing the frame rate from hundreds of Hz to kHz. However, one of the key differences between the two KLDT-E5TAs is that the manufacturer of the camera installed after 2019, which is Semiconductor Devices (www.scd.co.il/), only supplied a sensor integrated with a cooling unit and minimal driver & readout electronics; additional interface and power supply were produced by IPP Institute in Garching (Germany), (see [14]). Whereas in the case of FLIR (www.flir.co.uk/), which was the supplier for the first unit before 2019, a complete camera device was supplied.

There is a 25 mm diameter filter located within the KLDT-E5TA objective lens assembly, whereas the KLDT-P5TB system uses a filter mounted to the front of the lens which is 58 mm in diameter.

Figure 4 presents an image of the field of view obtained by the protection camera KLDT-P5TB. It is possible to notice two features on the image. Firstly, the noncircular shape of the edge of the field of view limit. This is due to slight clipping of the line of sight as it passes one of the mirror mount sides; it does not affect the specified field of view since it corresponds to another Tile 5 module. Secondly, within the image, there is a C-shape that looks like a water mark, which originates within the camera sensor (known because a previous camera device used initially for the same position does not show it). The horizontal and vertical axes are given in pixels. The grey scale colour map represents intensity levels labelled as 'counts'.

By comparing the CAD model (see figure 1) with the camera image (see figure 4) it is possible to observe that the

Table 1. List of DIR camera and viewing systems with application/s and wavelength range.

Viewing system ID & application	Wavelength range (μm)
KLDT-E5TA: temperature and heat fluxes for scientific purposes	3.1–4.7
KLDT-P5TB: in vessel protection via temperature measurements	1.25 ± 0.025
KLDT-E5PA, KLDT-E5PB, KLDT-E5PC and KLDT-E5PD: –Spot temperature measurement on Tiles 5 and 6 using pyrometers ($\times 2$) –Spectroscopy measurements ($\times 2$)	1.4–1.7

field of view is slightly smaller than the one shown in the CAD model. However, the result is still acceptable since the key objective was to view at least one complete module of Tile 5 as well as the other vertical tiles listed. Furthermore, comparing the field of view of the protection camera with the field of view produced by the mid-infrared camera KLDT-E5TA (see figure 5), it is possible to note that the field of view of KLDT-E5TA is slightly smaller than the one for the protection camera (KLDT-P5TB). The reason being that for the scientific camera the priority is the optimization of the visualization of stacks B, C and D from Tile 5.

The KLDT-E5TA camera using the Pelican-D sensor in the SemiConductor Devices camera has twice the spatial resolution because the pixel pitch is half that of the Titanium 550 FO InSb sensor in the FLIR camera. The axes are given in pixel units and the vertical grey scale represents intensity levels.

The images presented in this section obtained from JET pulses were produced with a software called JUVIL (see [15]). In addition, the image shown in figure 4 was obtained from a plasma disruption during the pulse in order to be able to reach sufficient plasma light to be able to confirm the image quality as well the alignment.

Completing the diagnostics on the DIR LOS, there is a set of fibre telescopes located near the edge of the limit of the LOS using space leftover by the two camera systems. The fibre telescopes are connected to two pyrometers and two spectrometers. The pyrometers are a two-colour digital type using narrow wavelength ranges centred at 1.53 μm and 1.66 μm. They have integrated visible lasers for back illumination to aid alignment. The manufacturer is Advanced Energy (www.advancedenergy.com/). The model is IGAR 12-LO (see [16]). The temperature range is 300 °C–3300 °C. The use of two wavelengths provides the advantage of making the calculation of the temperature independent of the surface emissivity of the tiles.

One of the pyrometers is connected to a fibre telescope with the addition of a single-to-stripe fibre bundle (commonly used for shaping fibre light to align with a spectrometer slit) so that it collects emission from three ∼40 mm diameter spots in a line along the Tile 6 extension (see figure 6).

The second pyrometer was aligned initially to cover stacks C and D on Tile 5 (i.e., approximately 120 mm diameter)
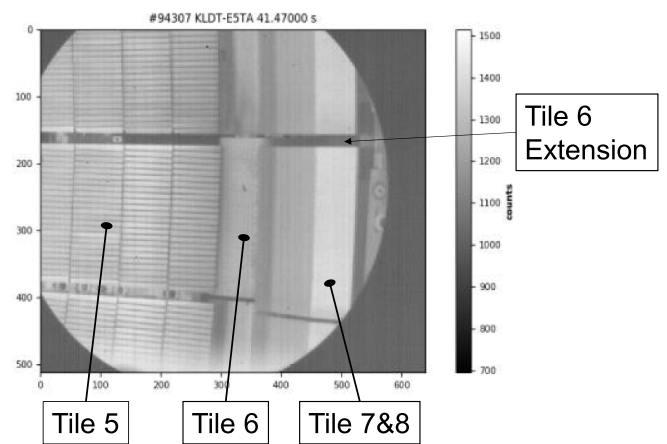
Table 2. Specifications of the DIR camera systems (FF: Full Frame).

Specification	KLDT-P5TB	KLDT-E5TA until 2019	KLDT-E5TA after 2019
	protection of in-vessel tiles	Scientific camera (temperature and heat fluxes)	
Pixel size	15 μm	30 μm	15 μm
Sensor size	640 × 512	320 × 256	640 × 512
		9.6 × 7.68 mm	
Sensor type	InGaAs	InSb	
Frame rate (Hz)	25 used 25–150	300 (FF)–8000	300 (FF)–3000
Exposure	100 μs–25 ms	1 μs–20 ms	
Digitization	14 bits	14 bits	13–15 bits
Interface	3.0 USB	Gigabit Ethernet	Camera Link
Cooling	Single stage Peltier	Stirling (77 K)	
Filter μm	1.250 ± 0.025	3.9 ± 0.8	
Dimensions (mm)	64 × 56.3 × 47.1	230 × 110 × 150	309.5 × 100 × 121.2
Weight (kg)	0.23	∼3	∼4.2
Model	WiDy SWIR 640V-ST	Titanium 550 FO InSb	Sensor: Pelican-D
Supplier	New Imaging Technologies (NIT)	FLIR	SemiConductor Devices
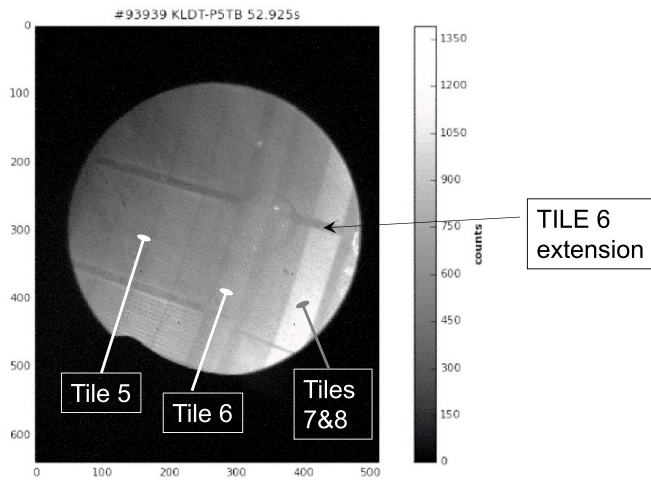
Figure 4. Image obtained from the protection camera (KLDT-P5TB) during JET pulse 93939.

Figure 5. Image obtained from the Pelican-D KLDT-E5TA camera for pulse 94307.

but the collection spot was too large, and the fibre telescope was then modified to receive emission from a spot that only covers the width of Stack D (approximately 60 mm diameter; see figure 7). The presence of intense reflections observed in the figure as bright saturated areas provides an illustration of the level of difficulty in the alignment of the pyrometers. Figure 7 has images with and without labels to facilitate the visualization of the back-illuminated spot location more easily.

The two remaining fibre telescopes, which are connected to spectrometers, are aligned with a single spot view covering stacks B and C of Tile 5 and of Tile 6 respectively.

5. Optical modelling

The requirement of the optical modelling was to design a relay system that could reproduce the field of view and image quality of the previous camera system located inside the Torus Hall and installed on top of one of the main upper vertical ports looking down into the divertor region of the vessel. Again, as with the WAV LOS, the addition of new optical components with associated optical losses means that it is not possible to achieve the same optical throughput. In this optical design, with the exception of the vacuum windows, all the components are new. The optical design was carried out using Zemax (www.zemax.com/) optical modelling software. The
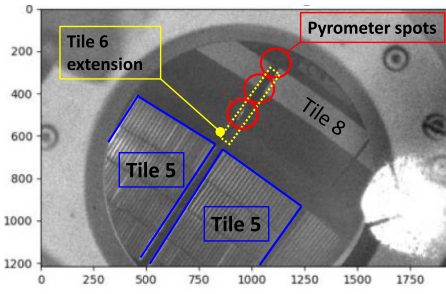
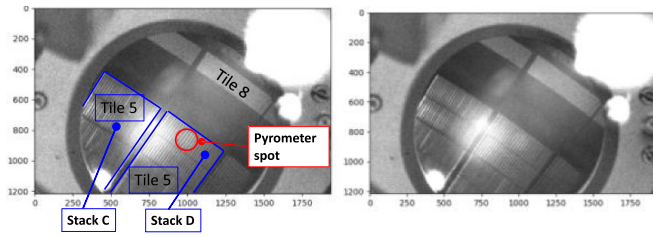**Figure 6.** Pyrometer back-illuminated spots on the Tile 6 extension.

Figure 7. Pyrometer back-illuminated spot-on stack D on Tile 5 with (left) and without (right) labels for better contrast.

manufacturing tolerances were also calculated using Zemax. The criterion used for the calculation of the critical parameters was the root mean square Spot Radius and the calculation used 1000 Monte Carlo cycles. This section is divided into four sub-sections: starting with the mirror relay and following with all the imaging optics for the camera systems and fibre telescopes.

5.1. DIR mirror relay

The DIR mirror relay consists of a total of six mirrors and one refractive element. It is used for relaying the light and thermal emission from the divertor tiles into the viewing systems (see figure 2 and table 1). Out of the six mirrors which are numbered according to the sequence of their positions in the relay path, four are located in the Torus Hall and they are denoted as M1-M4; the remaining two (i.e., M5 and M6) are fold mirrors and they are located in the laboratory adjacent to the Torus Hall on the other side of the biological shield, receiving light through the DIR penetration. The DIR penetration is next to the WAV penetration as discussed in [6]. Figure 8 shows Zemax raytracing images of the relay with close up views of the top of the machine and the camera lab listing all the optics (see [17]). The close view of the top of the machine comprises the following: a set of two vacuum windows inside the window tube and on top of the 'Upper main vertical port', there is a lens (L1) and two mirrors (M1 and M2) close together to reflect the light path towards the third mirror, M3, which then reflects the light path to M4. The light path is then directed from M4 towards the penetration in the biological shield into the adjacent building (J1F) where the final two relay mirrors, M5 and M6, are located along with the cameras and their optics.
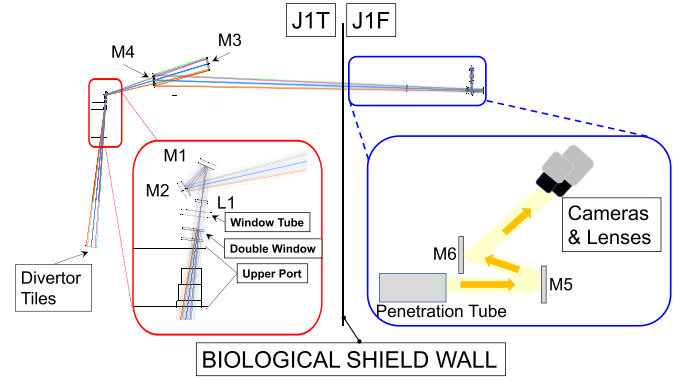

Figure 8. DIR Mirror relay showing the Zemax ray tracing (pyrometers are not shown).

Table 3. Some of the key parameters for optical relay components.

ID	Diameter (mm) +0.00/−0.25 mm	Thickness [centre] (mm) ±0.2 mm	Weight (kg) ± (0.01–0.1) kg
L1	50.0	10.0	0.97
M1	75.0	12.5	0.12
M2	100.0	19.0	0.33
M3	500.0	55.0	24.44
M4	500.0	12.0	23.65
W1	280.0	38.0	2.94
M5	250.0	38.0	4.09
M6	300.0	38.0	5.88

A list of the key parameters for each of the optical elements in the relay is provided in table 3. The lens is plano-convex and uncoated. The radius of curvature of the lens is 1800 mm. The lens and the penetration window are both made of sapphire. This table does not include the existing pair of vacuum windows inside the port as they are not new components, but they are also made of sapphire. However, the vacuum windows were included in the optical modelling. The mirrors are all made of fused silica substrates with enhanced aluminium coatings which provide a relatively flat level of reflectivity in the two wavelength bands used by the DIR diagnostics (see figure 11). All the mirrors are flat with the exception of M3 whose radius of curvature is −8590 mm.

The image quality of the relay was modelled using a paraxial lens with a focal length of 400 mm. The transfer optics design was optimised to be diffraction limited with an Airy radius of 12.3 μm at a wavelength of 4.0 μm. The through-focus-spot diagram shows the diffraction limited result in the central column of the graph (see figure 9 and [17]).

The modulus of the complex optical transfer function, also known as modulation transfer function (MTF), is provided in figure 10 and [17]. The maximum spatial frequency is achieved around 90 cycles mm^{-1} at a wavelength of 4.0 μm.

The tightest manufacturing constraints obtained with Zemax are first, the curvature error of 43 mm for mirror M3 which can be compensated with a mirror displacement of 30 mm although, in practice, all the required image adjustments were performed with the camera systems. Secondly, the flatness error of 4 fringes for mirror M6.
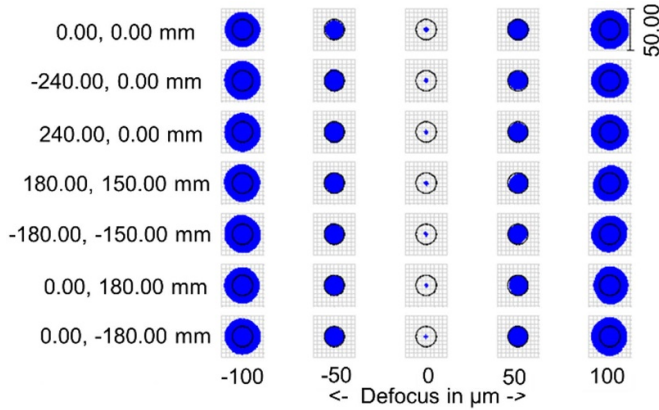
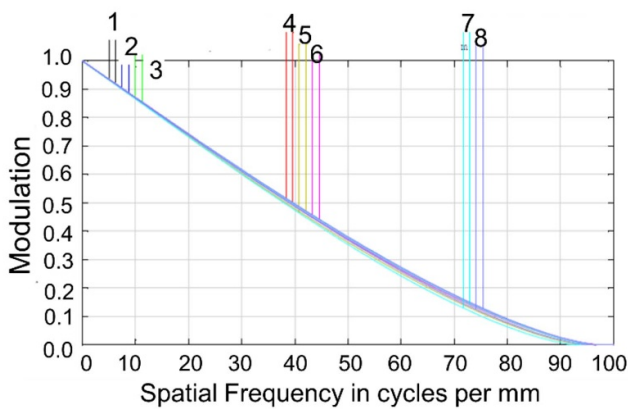**Figure 9.** Through focus spot diagram for DIR mirror relay.

Figure 10. Modulation transfer function for DIR mirror relay. The numbers at the top represent the tangential and sagittal cases as listed here: **1**: Diffraction Limit, **2**: 0.00, 0.00 mm, **3**: −240.00, 0.00 mm, **4**: 240.00, 0.00 mm, **5**: 180.00, 150.00 mm, **6**: −180.00, −150.00 mm, **7**: 0.00, 180.00 mm, **8**: 0.00, −180.00 mm.

Although M6 mirror is flat, since it is the last mirror in the relay, keeping the flatness error not higher than 4 fringes ensures the optical performance calculated by the optical model.

The estimated transmittance of the DIR relay is presented in figure 11 (black line). The contribution of different combinations of components involved in the relay are included as dashed lines: the double window inside the upper main vertical port, the lens L1 on top of the window pair, the mirrors M1–M6 as well as penetration window. The narrow dips in transmission between the wavelength range 2.5–2.7 μm are believed to be instrument artefacts in the spectra.

5.2. Imaging optics for the MWIR camera system KLDT-E5TA

There are two camera systems within the DIR LOS. The one described in this section is a MWIR camera system for the measurement of the heat fluxes and temperatures of the divertor tiles (see table 1). The objective has a focal length of 350 mm and a 120 mm diameter aperture (see [18]). It is achromatic and athermalized and all components are spherical. It provides the functionality of inserting an optical
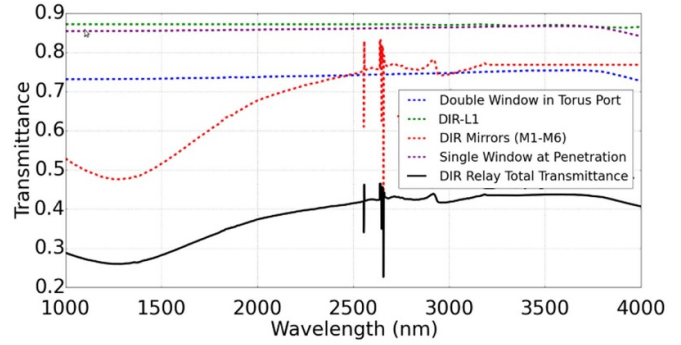

Figure 11. Estimated DIR relay Transmittance in the black trace. Dashed lines represent the estimated transmission of the main components: double window in Torus port (blue), L1 (green), single window at penetration (magenta) and estimated reflectivity from DIR mirrors (red).
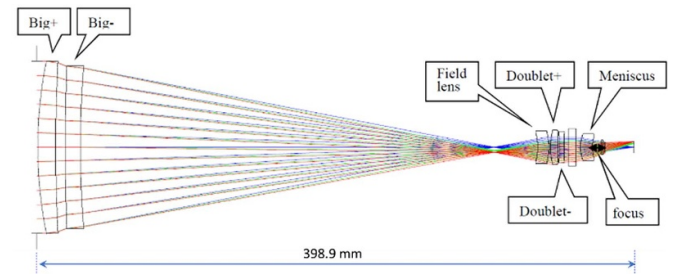

Figure 12. Schematic of the imaging optics for MWIR divertor camera (KLDT-E5TA).

filter between the element labelled as 'Doublet −' and the 'Meniscus' lens. A schematic showing the optical elements is in figure 12 (see [18]). The objective comprises six elements which have been given different names. All the optical elements are made with Silicon with the exception of the second and the sixth elements (i.e., 'Big −' and 'Doublet −') which are made from Germanium.

The through spot performance of this objective is presented in figure 13 (see [18]). The black circle represents the diffraction limit at a wavelength of 4 μm. The Airy radius is 13.96 μm. The spot size is smaller than the Airy disc. This is also applicable for other wavelengths such as 3.0 μm and 3.6 μm.

The MTF is close to the diffraction limit for the wavelength range from 3.0 to 4.0 μm (see figure 14) .

The key parameters of the individual elements are listed in table 4. The tolerancing exercise carried out in Zemax showed that the decentre of the Field lens was limited to 0.05 mm and the two Doublets (i.e., 'Doublet +' and 'Doublet −') to ±0.1 mm in order to maintain the overall imaging performance.

5.3. Imaging optics for the protection camera KLDT-P5TB

The imaging optics of the protection camera shares the same light path footprint as the MWIR camera. Sharing the light footprint is advantageous as a concept of extending the diagnostics capability. Specifically for the protection camera, the
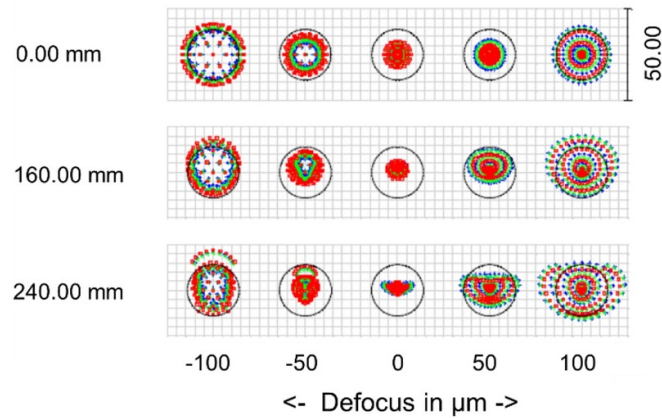
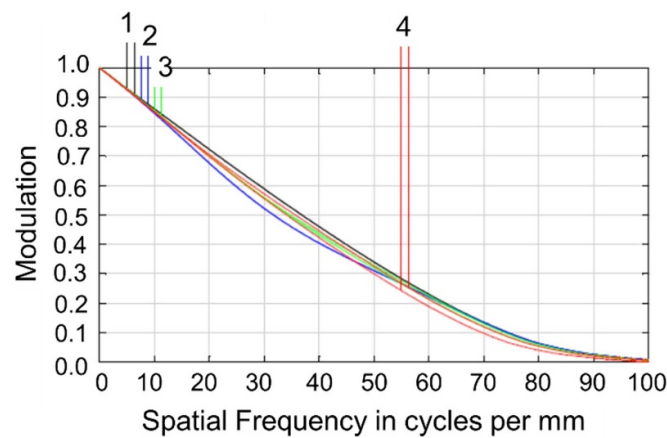**Figure 13.** Through spot diagram for the objective of the middle infrared divertor camera KLDT-E5TA.

Figure 14. Modulation transfer function for the objective of the middle infrared divertor camera (KLDT-E5TA). The numbers at the top represent the tangential and sagittal cases as listed here: **1**: represents the diffraction limit, **2**: 0.00 mm, **3**: 160.00 mm, **4**: 240.00 mm.

Table 4. Design Tolerances for the objective of the middle infrared divertor camera KLDT-E5TA.

Element (material)	Radius (mm)	Thickness (mm)	ClearAperture diameter (mm)
Big + (Silicon)	287.4 cx 1075.00 cc	12 ± 0.1	116 113
Big − (Germanium)	1945.51 cx 633.98 cc	10 ± 0.1	109 106
Field (Silicon)	−32.89 cc −37.01 cx	7.5 ± 0.05	18 22
Doublet + (Silicon)	43.74 cx −243.9 cx	5 ± 0.05	23 22
Double − (Germanium)	−111.5 cc 152.96 cc	3 ± 0.1	21 20
Meniscus (Silicon)	23.50 cx 23.50 cc	8.0 ± 0.1	18 13

imaging optics is an optical lens which is only partially filled (note the area of the lens front which is out of the LOS viewing area is not obscured because no contribution from parasitic light was found). The light path diameter specified for the scientific MWIR camera is 192 mm whereas the aperture needed for a good quality image for the protection camera is approximately only 38 mm.

The objective lens used is manufactured by Canon with a focal length zoom range of 75 mm–300 mm (model number EF75300); the *F*-number varies from ƒ/4 to ƒ/5.6 for this
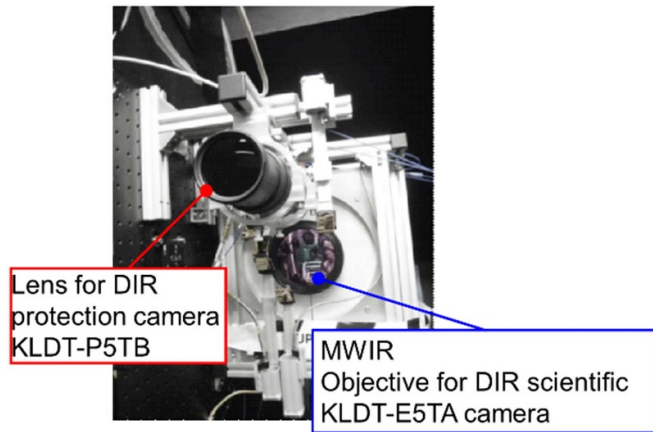
Figure 15. Positional layout of the Canon lens for the protection camera in DIR (KLDT-P5TB) and the front surface of the MWIR objective for the scientific camera KLDT-E5TA.

zoom range (see [19]). The operational focal length used was 300 mm. This lens is used with a C-mount adaptor. The physical diameter of the lens is 71 mm. Although it is not mentioned in the data sheet, it has been found that the lens performs well for the near infrared region (where there is risk of severe internal reflections depending on the performance of AR coatings so far outside their normal wavelength range). According to figure 11, the DIR relay transmittance around the wavelength region used by the protection camera is less than 30%. However, this has been found to be sufficient light to produce a useful image for protection. This was possible due to the high quantum efficiency of 70% of the protection camera using an InGaAs sensor. In addition, this performance is similar to the protection camera systems installed in the Torus Hall which use shorter wavelengths close to the upper limit of the silicon sensors used (see [20]).

Figure 15 shows a photo of the positional layout of the Canon lens for the protection camera system (KLDT-P5TB) and the MWIR objective for the scientific camera sharing the DIR LOS.

5.4. Fibre telescopes for spectroscopy applications

Four fibre telescopes were designed to be coupled into two spectrometers and two pyrometers as mentioned in section 4. Similarly, as the optical lens used on the protection camera (see section 5.3), the fibre telescope also shares a section of the light path footprint. The key features of the common design of the fibre telescope are shown in figure 16. A gold coated steering mirror reflects the light into a short tube towards a concave mirror. In turn, the light reflected from the concave mirror is focussed into the fibre optic which then connects at the other end to either a pyrometer or a spectrometer. The fibre diameter and focal length of the concave mirror determine the size of the image spots in the divertor.

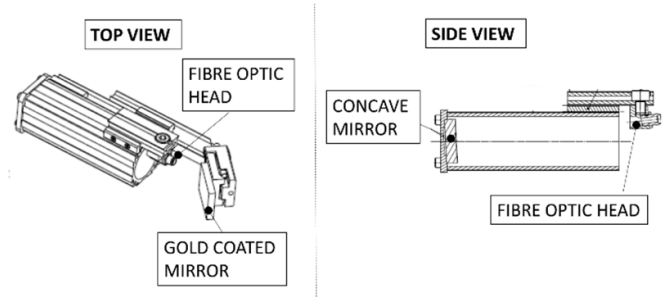A photo of the four fibre telescopes together with the protection camera KLDT-P5TB and the scientific MWIR camera

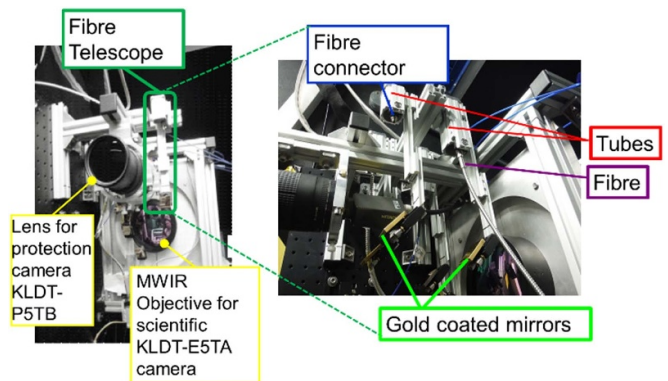
Figure 16. Key features of the fibre telescope.

Figure 17. Photo showing the location of the fibre telescopes in between the Canon lens of the protection camera (KLDT-P5TB) and the MWIR objective. Parts shown on figure 16 are also labelled in the photo.

(KLDT-E5TA) is presented in figure 17. They are located next to the optical lens of the protection camera and just above the MWIR objective of the scientific infrared camera.

6. Engineering design of the DIR mirror relay in the Torus Hall

This section describes the mounting and support structures of the optical relay in the Torus Hall. The main requirement for the design was to ensure that the structures were sufficiently rigid to avoid any physical deformation or movement which could alter the optical alignment. This was particularly critical during the D-T campaign since access to the Torus Hall was severely restricted due to neutron activation. The relay inside the Torus Hall comprises three optical mounting assemblies which are known as DIR-L1-M1-M2, DIR-M3 and DIR-M4 assemblies. All these mounting assemblies have the same name as the mounting optics following the sequence of the optical path. The text will distinguish between the optic as a component and the mount assembly. In addition to the description of the mechanical design, the engineering analysis for each of these mirror assemblies is also included here. The most novel part in this overall system design, as it was with the WAV system (see [6]), is the design and installation of two large bespoke kinematic mirror mounts made of GRP material for mirrors M3 and M4 (both 500 mm diameter). Due to the large size of the mirrors and the potential for eddy currents during
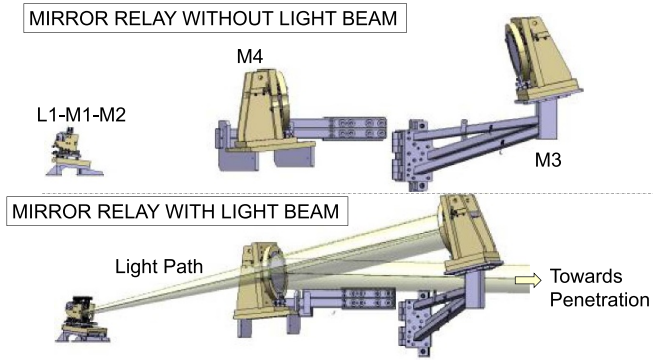
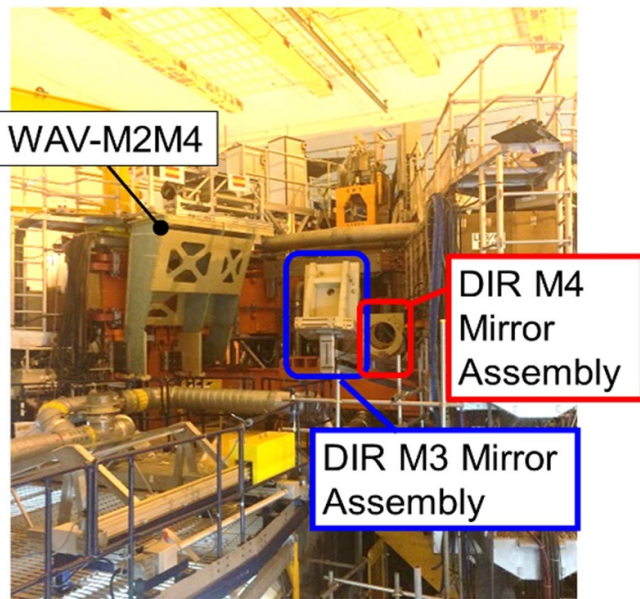**Figure 18.** All mirror assemblies with and without the light path.

Figure 19. Photo of the installed M3 and M4 mirror assemblies.

the JET pulse, it was not possible to use a commercial off the shelf (COTS) mount design. One important difference with the WAV system (see [6]) is that these two custom kinematic GRP mirror mounts were fixed vertically. Figure 18 shows a CAD model image of all the mirror assemblies with and without the light path.

A photo of the installed M3 and M4 mirror assemblies inside the Torus Hall is provided in figure 19. The installation area is quite congested, hence the reason for showing the models is for a clear view of the DIR mirror assemblies. One of the mirror assemblies from the WAV LOS, WAV-M2M4 is also visible in the photo.

6.1. DIR L1-M1-M2 mirror assembly

The L1-M1-M2 mounting assembly is installed on top of the machine directly onto the upper main vertical port in octant 5 over the vacuum window. The assembly contains three optical elements: a lens denoted by L1, mirror M1 and mirror M2 (see figure 20).
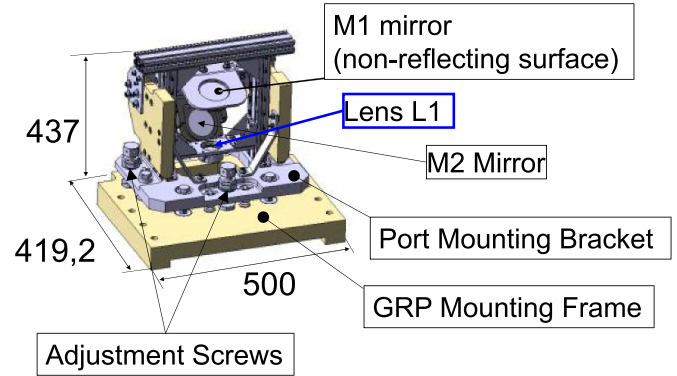

Figure 20. Front view of the DIR-L1-M1-M2 assembly noting overall dimensions in millimetres and key components.

Components which have been coloured in yellow represent the parts that are made from GRP whereas the blue colour represents metal parts. Since sections 4 and 5 described the specifications of the optical components in detail, only the main characteristics will be mentioned briefly here: lens L1 is a plano-convex lens of 50 mm diameter made of sapphire, M1 mirror is a flat mirror with diameter of 75 mm and M2 is the second flat mirror with a diameter of 100 mm, both are made of fused silica.

The overall dimensions are also listed in figure 20. The total weight is 50.22 kg. In addition, the figure lists the key components visible on the front side of the assembly, including: the 'GRP Mounting Frame' assembly, the 'Port Mounting Bracket' fitted on top of the 'GRP Mounting Frame' assembly, the two side plates for the left and right-hand sides and the lens bracket which goes horizontally joining both sides. The two mirrors (i.e., M1 and M2) form an angle of approximately 35° in order to provide behaviour like a 'corner cube configuration' but for the required system light path angle between the port axis and the axis from L1-M1-M2 assembly to mirror M3. The reason for using two mirrors in this corner cube configuration was to eliminate the effect of tilts and displacements due to movement of the machine during the pulse.

6.1.1. GRP mounting frame. Starting from the 'GRP Mounting Frame', this was installed and supported by the vacuum port flange structure (see figure 26). The assembly consists mainly of the GRP plate made of EPM203 (see [21]). The shape of the GRP frame has been adjusted to fit around the vessel structure at this location. However, this GRP mounting plate cannot be described in isolation because this component together with the 'Port Mounting Bracket' form a kinematic mount for the three optical elements as a group (i.e., lens L1, M1 and M2 mirrors). For the kinematic mount, there are three kinematic receiving contact parts which are referred to as: 'Cone', 'Vee' and 'Flat' (see figure 21). This ensures that each degree of freedom is constrained only once, thus avoiding over-constraint.

The adjustment screws (see figure 20), which are within the 'Port Mounting Bracket', are installed to make contact with the special kinematic receiving contact parts or 'feet' (see
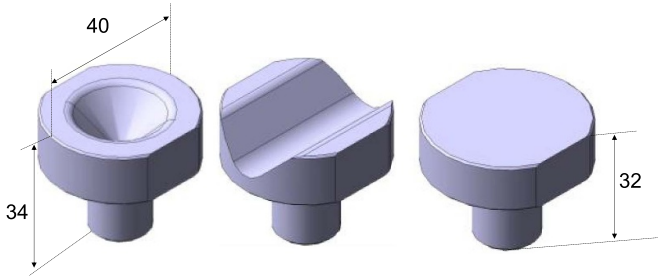
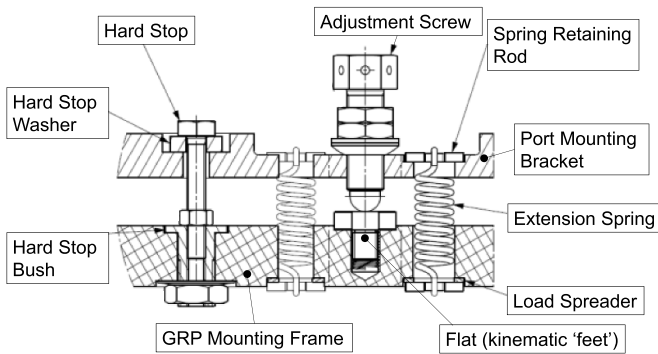**Figure 21.** Kinematic receiving contact parts or kinematic 'feet': Cone (left), Vee (middle) and Flat (right).

Figure 22. Cross section as example of the adjustment screws. This figure shows specifically the 'Flat' kinematic feet.

Figure 23. Side view of L1, M1 and M2 including the light path (thick blue line) with one of the side plates removed.

figure 21). The three adjustment screws are positioned in a triangular shape which allows the whole L1-M1-M2 assembly to be tilted by the 'Port Mounting Bracket' moving relative to the 'GRP Mounting Frame'. A cross section of one of the three adjustment screws with one of the kinematic 'feet' such as the 'Flat' one, is provided in figure 22.

The adjustment screws each have a hardened steel 'Adjustment Ball' inserted in the end for interfacing with the kinematic feet surfaces. The dimensions of each adjustment screw are 102.2 mm × 41.6 mm. The adjustment ball has a radius of 20 mm. On both sides of each adjustment screw there are two springs (see figure 22) to hold the 'Port Mounting Bracket' and 'GRP Mounting Frame' assemblies together and provide sufficient tension if the DIR L1-M1-M2 assembly moves or vibrates during a JET pulse, since the assembly is being supported by the vessel itself (see figure 1). Within the 'GRP Mounting Frame' assembly, a load spreader plate made from stainless steel has been inserted to distribute the action of the spring evenly. In case of an extreme case plasma disruption causing severe sudden movement of the assembly, there are fixing bolts which join the 'Port Mounting Bracket' to the 'GRP Mounting Frame' assembly (see figure 22). These fixing bolts are fitted with pre-loaded silicone rubber washers set after system alignment to act as 'hard stop' backups to the springs.

6.1.2. Port mounting bracket. The 'Port Mounting Bracket' is the base for the strut profile frame, which the side plates, the L1 mounting (see figure 20) and the mirror mounts are fitted
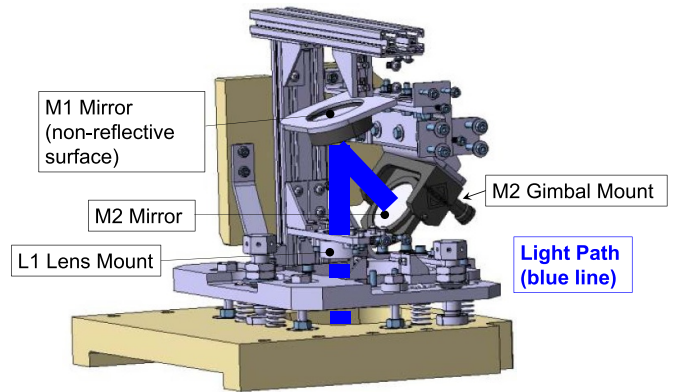
to. The strut profile frame structure and the steel base plate have electrical isolations to prevent eddy currents around the major structure shape.

6.1.3. Mounting of Lens L1, M1 and M2 mirrors. The optics are mounted from an aluminium extrusion frame subassembly in combination with stainless steel and GRP for stiffening and isolating, with braces to increase rigidity. L1 is held in a lens mount which also holds the system aperture. M1 is in a lens tube (not adjustable) and M2 is mounted in a COTS gimbal mount (see figure 23).

6.1.4. Engineering analysis. The engineering analysis consists of several types of calculations which includes the static deformation (see [22]) as well as the harmonic analysis (see [23]) of enhanced radial field amplifier (ERFA) kicks (see [24]). As mentioned also in [6], ERFA kicks, used in some JET experiments, are periodic voltage pulses applied to the radial magnetic field circuit causing magnetic field changes that perturb the plasma vertical position. Their periodic nature has the potential to cause vibration and excite resonances in mechanical assemblies. A summary of the key conclusions is reported here. The DIR-L1-M1-M2 assembly was analysed for the disruption case using a quasi-static approach as per standard JET practice, assuming an acceleration of 3.5 g in the radial direction, 2 g for the toroidal axis and 2 g for vertical axis. The worst-case reserve factors (RFs) at the kinematic feet contacts (see figure 21), considering the Hertzian stresses at the 'flat' contact, were 1.1 and >4 for shear stress and surface tearing respectively. The RF obtained for the surface tearing case was larger than 4 which represents a satisfactory result (RF = allowable stress/applied stress and RF > 1 is considered acceptable under worst-case disruption loads). The marginal RF for shear stress was also acceptable because only a few disruptions of the worst-case severity are anticipated for the remaining JET experiments; and exceeding the allowable shear stress would only be predicted to result in a minor surface indentation, which could be mitigated by a re-alignment of the optics if necessary.
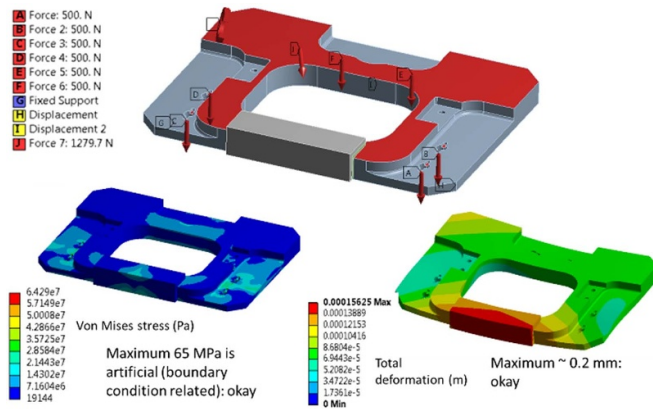
Figure 24. Analysis model showing static stresses and deformations in 'Port Mounting Bracket' (see [22]).

Furthermore, the disruption RF for the bolts securing the vertical strut to the base plate is larger than 3 which again means it is fit for purpose. The associated maximum bending stress in the vertical strut is less than 25 MPa which is considered acceptable.

The corresponding stresses in the stainless steel 'Port Mounting Bracket' are illustrated in figure 24. The model used for the 'Port Mounting Bracket' appears at the top of figure 24. In addition, to consider the case for the worst-case disruption, it is also included that the spring forces required are 500 N. The red arrows in figure 24 show the forces applied which, as illustrated on the figure, are applied downwards to pre-load the assembly against the 'GRP Mounting Frame'. The kinematic feet, to which the correct kinematic boundary conditions are applied, are not visible because they are merged with the plate itself in the model. The stress and deformation levels are provided in the two bottom graphs. The bottom left-hand side graph shows the simulated results for the stress levels, where the colours represent different levels of the von Mises stresses. The maximum value quoted on the graph of 65 MPa is considered artificial due to boundary conditions imposed in the model. Thus, the overall stress levels for the worst-case disruption are valued as acceptable.

The associated deformation level, shown in the bottom right-hand side of figure 24, is calculated to reach a maximum of 0.2 mm which again is deemed to be acceptable. Similar modelling was carried out for the 'GRP Mounting Frame'. The value of the spring forces included in the model were again 500 N. The associated deformations were again deemed acceptable. Note that an optimisation exercise was performed on the springs (see [25]), resulting in the installed spring force being somewhat lower than the 500 N assumed in the analysis, but still sufficient to hold the feet down in all but the 20 worst anticipated disruptions for the remaining lifetime of JET. There are six 'hard stops' in the assembly that prevent significant separation (effectively a second set of stiffer springs) and maintain foot contact for these worst cases.
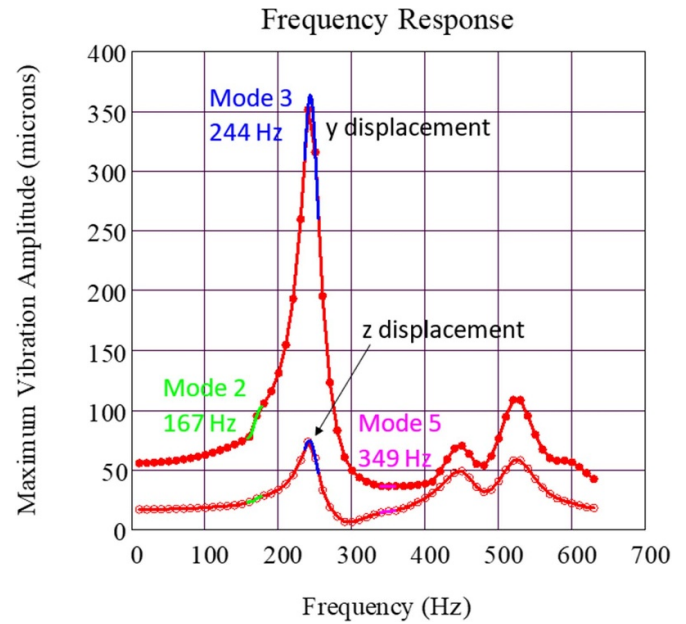

Figure 25. Harmonic analysis of the DIR-L1-M1-M2 assembly depicting the different modes as a function of amplitude in metres for mirror M2. The red trace represents a course scan of 10 Hz resolution. The green trace represents a fine scan of 1 Hz around 167 Hz. The blue trace represents a fine scan of 1 Hz around 244 Hz and the pink trace represents a fine scan of 1 Hz around 349 Hz (see [26]).

The assembly was analysed for the impact of ERFA kicks, which can generate eddy current torques in the mirror mounts and the different parts of the assembly. The model used for the harmonic analysis does not include 'GRP Mounting Frame' because it is not affected by eddy currents and is considered to be a rigid base. In addition, the M1 and M2 mirrors have been replaced by point masses in the model for simplicity. The eddy current torque for L1 has conservatively been assumed to be the same as for mirror M2. A typical frequency response in this case for mirror M2 is shown in figure 25 (see [26]). The harmonic analysis results are shown for two axes of displacement: *y* and *z*, with the inclination of the mirror lying between these two axes. The amplitude plotted in each case is the maximum vibration amplitude over one of the annular surfaces of the inner gimbal ring, which is thus representative of the behaviour of the M2 mirror enclosed by the ring. The assumed level of damping is 5%. The accompanying WAV system paper (see [6]) considers the validity of this damping assumption, concluding that it is likely to be overestimated. Some undamped natural frequencies of the assembly are also indicated, obtained from a separate modal analysis.

Three different modes of concern have been identified to which the ERFA excitation is well coupled: mode 2, mode 3 and mode 5 (see figure 25). 'Well coupled' here implied that some aspect of the mode shape is consistent with the deformation generated by the ERFA excitation. These modes represent natural frequencies which are for mode 2: 167 Hz, for mode 3: 244 Hz and for mode 5: 349 Hz. The curves are coloured

Table 5. Sensitivity of L1-M1-M2 assembly to rotations about various axes.

Rotate about	Rotation	Image displacement	Displacement/degree
Case: To represent whole port tilting			
Top of window assembly	0.5°	65 μm	130 μm/°
Case: To represent coupled M1-M2 rotation			
Roughly where M1 and M2 pivot	0.5°	~65 μm	~130 μm/°
Case: To represent differential M1-M2 rotation			
Front surface of M2	0.05°	~40 μm	~800 μm/°

Requirements from Zemax Tolerancing:
–Differential mirror tilting to be below 0.07°
–Coupled mirror tilting minimises the beam deviation (0.5° maximum)

differently depending on the resolution of the scan, with the red curve being a coarse scan over a wide frequency range and the other colours being fine scans of ± 10 Hz range about the various natural frequencies. As a result of these modes, the assembly is predicted to move in different directions and forms during ERFA kicks. For mode 2, the entire assembly can swing backwards and forwards as if 'nodding' which also includes swinging movements of the two mirrors, although these latter movements are not consistent in phase with the 'nodding' with regard to the ERFA excitation. The two mirrors can move in phase for mode 3, where the coupling to the ERFA excitation is highest, and antiphase for mode 5, where again there is phase inconsistency between the motions with regard to the ERFA excitation and thus lower coupling. Finally, there is another mode (mode 1), which is not shown in the graph; this corresponds to sideways movement, but this mode is not well coupled with the ERFA excitation. Displacements predicted by the harmonic analysis were converted into angular rotations of the optical elements. This required determining the displacements normal to the mirror surface of diametrically opposite points on the inner gimbal ring. The results of figure 25 do not directly correlate with mirror rotation because it is possible for the mirror to vibrate without any rotation. The sensitivities in terms of image displacement for a given rotation are listed in table 5 for three different rotation cases, together with the rotation limit requirements (see [27]). Table 5 shows that the assembly is most sensitive to differential rotation between mirrors M1 and M2. The corner cube arrangement of these mirrors meant that they were significantly more tolerant to coupled rotation (see table 5).

Table 6 presents the predicted worst-case coupled and differential rotations of mirrors M1 and M2 during ERFA kicks (see [26]). All the values are within the target with the exception of mode 5 for the case of M1-M2 differential movement, where the predicted figure is $\pm 0.042°$. Some analysis-based tuning of the geometry had been performed to meet the mode 2 and 3 targets and given the project timescales, the 20% excess differential rotation for mode 5 was accepted. Note that, since the mirrors move largely in-phase in mode 3 and out-of-phase in mode 5, smaller amplitudes of individual mirror vibration in mode 5 result in larger differential rotation for mode 5 than

Table 6. Predicted worst-case coupled and differential rotations of mirrors M1 and M2 during ERFA kicks from harmonic analysis.

Mode	M1-M2 coupled (goal = $\pm 0.25°$)	M1-M2 differential (goal = $\pm 0.035°$)
2	$\pm 0.04°$	$\pm 0.028°$
3	$\pm 0.15°$	$\pm 0.030°$
5	0	$\pm 0.042°$

for mode 3. This, together with the lack of direct correlation between maximum vibration amplitude and mirror rotation, explains why the mode 5 differential rotation is higher than that of mode 3, despite mode 3 dominating the mirror M2 frequency response in figure 25.

In summary, with careful design of electrical isolations to minimise eddy current loops and by combining electrically insulating materials with more commonly used metal mechanical engineering materials, it was possible to design an assembly for the optics with sufficient predicted stability despite the high (and sometimes rapidly changing) magnetic field in the installation position.

6.1.5. Installation of DIR L1-M1-M2 assembly. The total weight of the assembly is 50.22 kg, a lifting frame was required to transport the assembly and accurately lower it into position in the Torus Hall (see figure 26).

6.2. DIR-M3 mirror assembly

This is the second mirror assembly in terms of the optical relay light path. The assembly is attached to the transformer limb 5/6 in octant 5. Figures 2 and 18 illustrate the position of this assembly within the light path.

The overall dimensions of the DIR-M3 assembly are approximately 2.2 m in height and slightly less than 2 m in length. It can be divided into two sub-assemblies (see figure 27):

- Mounting Arm Assembly (including the hinge).
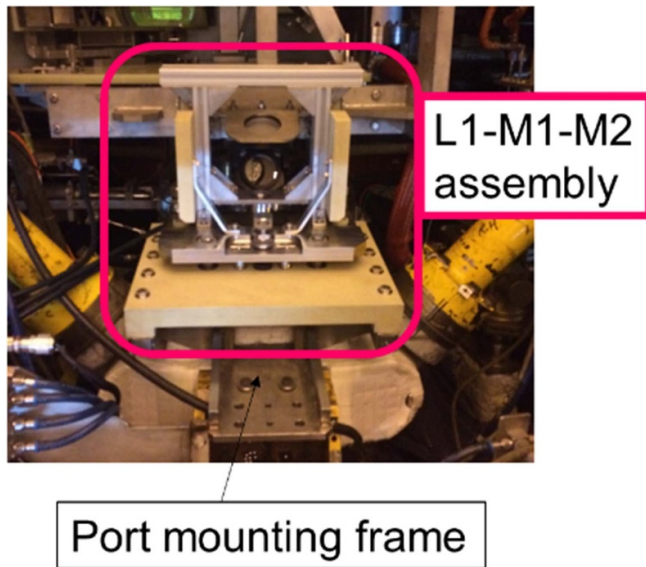- Kinematic mirror mount.

Figure 26. Photo of DIR-L1-M1-M2 after being installed in Torus Hall.
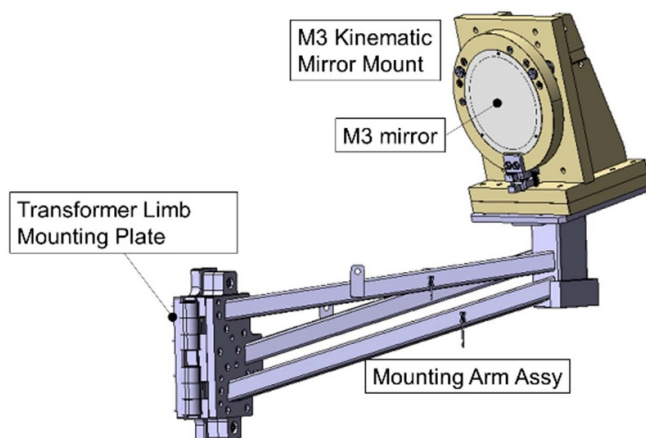

Figure 27. DIR-M3 assembly pointing the main sub-assemblies.

Each of these sub-assemblies will be described below in a separate section.

6.2.1. DIR M3 mounting arm assembly ('TV stand'). The 'Mounting Arm' assembly consists of the isolating 'M3 Mirror-Mounting Plate' assembly and the 'Mounting Arm' assembly (see figure 28).

The difference in colour presented in figure 28 represents the different materials used in this sub-assembly. The light orange colour represents the GRP type EPM203 (see [21]) and the rest of the components are made from non-GRP materials. The 'M3 Mirror-Mounting Plate' is the base platform of the M3 kinematic mirror mount.

Secondly, the 'Mounting Arm' assembly has the function of supporting the M3 mirror in the position required from the optical design. It is commonly known as the 'TV stand' because of its resemblance to a bracket used for this purpose.
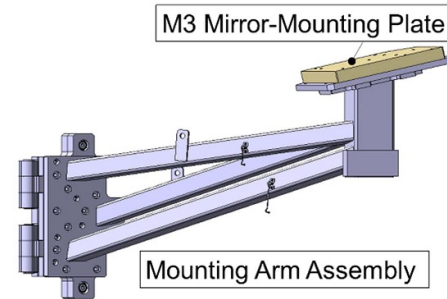

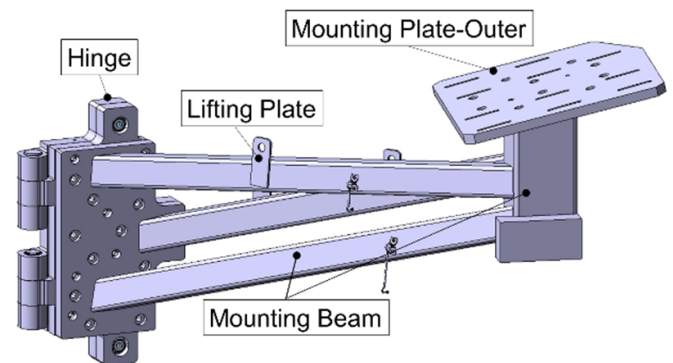**Figure 28.** Model depicting the mounting arm and plate assemblies.

Figure 29. Model depicting the main sub-assemblies of the 'mounting arm' assembly.

This type of structure, which is a cantilever, needs to be strong enough to support itself and the mirror mount while being rigid enough not to flex or vibrate. In addition, it has to remain stable in the presence of high and rapidly changing external magnetic fields (see [24]).

The mounting arm is fixed to the transformer limb using two plates where one of them is an insulating plate (see figure 30) made from EPM203 (see [21]). The insulating plate has the function of electrically isolating the assembly from the transformer limb, as is usual JET practice for attached electrically conductive sub-assemblies.

Figure 29 shows the main parts within the 'Mounting Arm' assembly: hinge, mounting beams, mounting plate-outer and lifting plate. The hinge assembly has the overall dimensions of 830 mm × 517.5 mm × 110 mm. The weight of the hinge assembly is 226.3 kg. The hinge has the capability of top and bottom 'Location Pins' which make the close position more precisely repeatable after opening and closing. As for the 'TV stand', the total weight without the hinge is 200.66 kg.

In addition, there is another level of complexity within the 'Mounting Arm' assembly, which is the capability to move the M3 mirror between two positions referred to as: operational and shutdown positions. The operational position is with the hinge closed and the shutdown position is with the hinge open (see figures 29 and 30). The shutdown position is required to enable the installation and removal of the remote handling tent for the installation of the JET servo-manipulator (MASCOT) (see [28]).
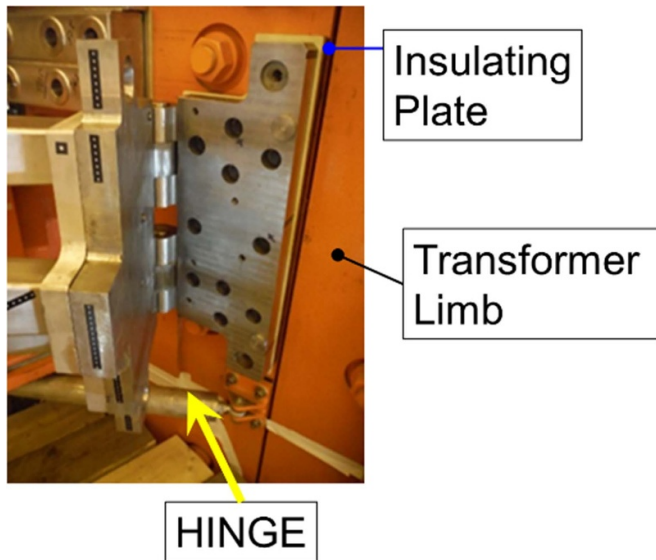
Figure 30. Photo taken during the installation of the assembly of the hinge fixed to the transformer limb. The hinge is shown in the open position. The insulating plate sandwiched between the hinge and the transformer limb is also shown.

All three mounting arm beams are hollow and welded at both ends. The vertical 'Mounting Beam' acts as a base for the optics assembly. This component is covered at the bottom end with a thin plate of 5 mm thickness which provides a base for the vertical 'Mounting Beam' and increases its torsional stiffness (see figure 29).

The 'Mounting Plate—Outer' includes a number of slots to provide sufficient flexibility in the adjustment of the M3 mirror position. There are also a number of lifting plates to be used during the installation. The opening and closure of the hinge was done with two operators lifted up by a mobile elevated working platform (MEWP).

6.2.2. DIR M3 mirror mounting assembly. The M3 mirror mounting assembly consists of a kinematic mirror mount that provides two functions: holding the mirror in place and the adjustment capability to precisely align the mirror angle. The loads predicted to be induced by eddy currents in the metallic mirror mount of the size required were considered significant enough to reject using a metal mount and instead produce an in-house design using GRP, but equivalent to a standard kinematic type of mirror mount. This had to be designed in house as no suppliers were found willing to undertake the design and fabrication of this type of mount. Figure 31 shows the two main sub-assemblies which are 'M3 Mirror-Mounting-Plate' assembly and 'M3 Mirror-Floating Ring' assembly. In addition, it also shows the two kinematic mirror adjustments with the 'Vee' and the 'Flat'. In addition, there is a kinematic constraint which is the 'Cone'. Starting with the 'M3 Mirror-Mounting-Plate' assembly, this comprises the majority of the components of the complete M3 mirror mounting. All the materials are made of EPM203 (see [21]) except the 'Pivot Pin Bracket' assembly (see figure 32) and the mirror adjustment bolts and the fixings.
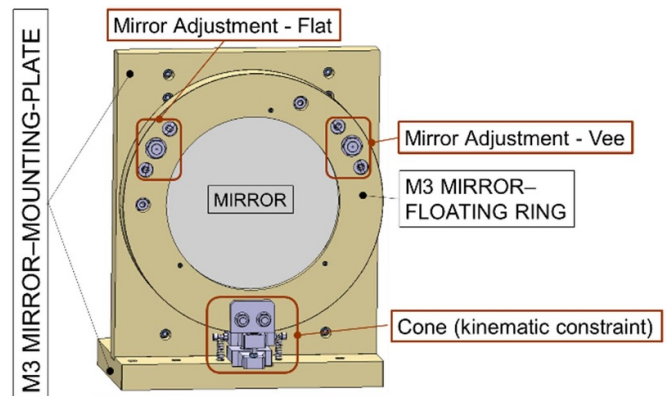

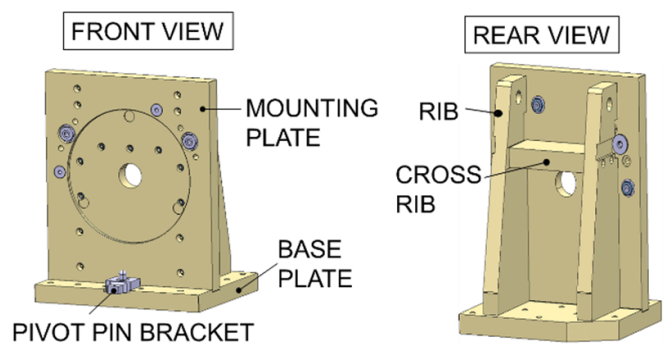**Figure 31.** Front view of the M3 Mirror mounting assembly.

Figure 32. Front and rear view of the M3 mirror mounting listing the key parts.

Figure 32 shows the different components with the front and rear views. The 'Base Plate' interfaces with the 'Mounting Arm' assembly (see section 6.2.1) and thus, serves as a base for the rest of the components. The dimensions are 720 mm × 550 mm × 70 mm.

The second component will be the 'Mounting Plate' assembly (see figure 32). The overall dimensions are 845 mm × 720 mm × 70 mm. The length dimension includes the studs used to fix the 'Mounting Plate' to the 'Base Plate'. The larger circular recess is relief to accommodate the back of the mirror itself—it has a diameter of 535 mm. The smaller diameter hole is 100 mm. The function of the smaller hole is there to show a portion of the back of the M3 mirror. This was considered a useful feature in case of the need to verify if the mirror had fallen out of the mirror mount during the D-T campaign, (since access to the Torus Hall was severely restricted), as this hole is visible through the penetration from the camera lab outside the Torus Hall.

There are different hole sizes for the fixing of each of the ribs and the adjustment screws. Figure 32 also presents the two ribs joined by a cross rib in order to provide stiffness.

The final component is the 'Pivot Pin Bracket' assembly which forms the base for the interface with the 'Cone' (see figure 32). This assembly consists of two components: 'Pivot Pin—Mounting Bracket' and 'Pivot Pin' assembly (see figure 33).
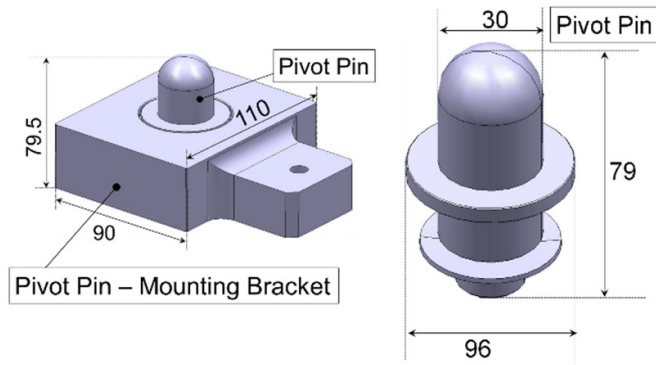
Figure 33. Left: 'Pivot Pin-mounting bracket' assembly which is attached to the 'baseplate' (see figure 32). Right: 'Pivot Pin' assembly. Dimensions in millimetres.
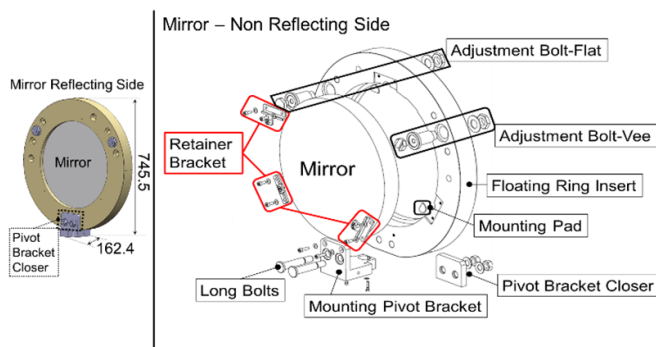

Figure 34. Left: front view of the floating ring assembly with dimensions in millimetres. Right: exploded view of the floating ring insert assembly, mirror and other key parts mentioned in the text. This right-hand side of the image has been enlarged for visualization purposes.

Figure 35. Diagram showing the generic adjustments provided in a standard kinematic mount using the three contact points (i.e., cone, vee and flat) (see [29]).

Figure 36. View of the Vee foot on its own (bottom left picture) with dimensions in millimetres and inside a close up of the Floating Ring assembly.

The 'Pivot Pin—Mounting Bracket' is a single component of material stainless steel 316Lgrade (see figure 33). The main feature of the mounting bracket is the hole in the middle with a diameter of 52 mm which is where the 'Pivot Pin' fits in.

Next, the 'Floating Ring' assembly is explained below. This is the component that holds the mirror and provides the adjustments to angle the position of the mirror to optimise the light path delivery within the rest of the mirror relay. Figure 34 displays the exploded view of the front and back view of the 'Floating Ring' assembly with all the main components listed. The mirror is being held at the front by the floating ring component since the aperture at the front is smaller than at the back. The 'Floating Ring Insert' assembly is the ring where the mirror sits. The front aperture has a diameter of 477 mm, whereas the aperture at the back (the side used to install the mirror) has a diameter of 502.5 mm. The weight of the 'Floating Mirror Insert' is 26.6 kg. There are three 'Retainer Brackets' positioned in a triangular shape whose purpose is to secure the mirror and prevent it from falling out of the floating ring. The top of the bracket is the part that connects to the mirror via a Nylon tip screw of M10 size. The reason to use a Nylon tip is to prevent any damage of the non-reflecting mirror surface when applying pressure to hold the mirror in position.
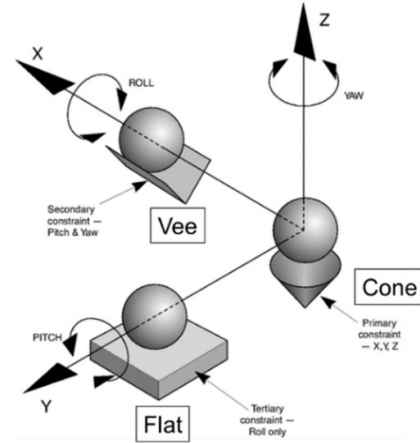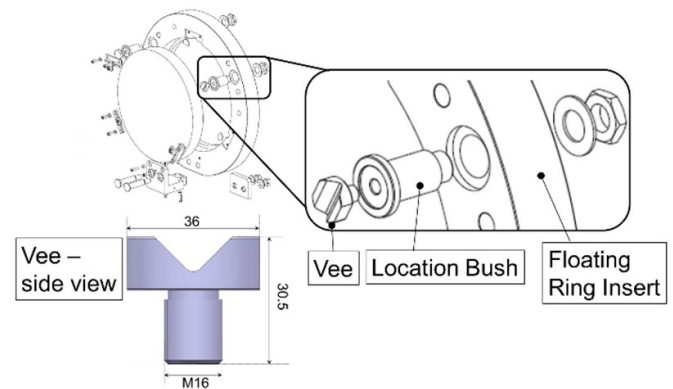
The mirror is sandwiched between the 'Retainer Bracket' and the 'Mounting Pad'. The shape of the pad is depicted in figure 34. There are three mounting pads located on the 'Floating Ring Insert' sitting at 120° from each other on the circular step directly below the 'Retainer Bracket' assembly as shown in figure 34.

In this kinematic mount, there are two types of adjustments: 'Adjustment Bolt-Vee', 'Adjustment Bolt-Flat' and one constraint—the 'Cone Bracket'. These three contacts form a triangular shape, and they provide the capability to tilt the position of the mirror in order to optimize the image performance. Comparing with standard kinematic mount, see figure 35 (see [29]), the 'Vee' and the 'Flat' contacts are in our case in the vertical plane since the mirror is standing vertically and they are also both connected to the adjustment screws.

Figure 36 shows a close up of an exploded view of the 'Adjustment Bolt-Vee' inserted into the 'Floating Ring Insert' using a location bush and some fixings. In addition, a side view of the 'Vee' interface with key dimensions is also included.
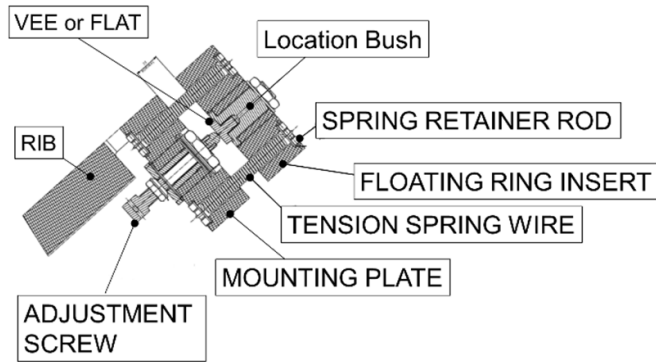
Figure 37. Top view cross section of the Vee or Flat 'Adjustment Screw' assembly listing the main components.

Figure 38. Cross section showing the 'Mounting Pivot Bracket' and 'Pivot Pin' within the 'Floating Ring Insert' and the 'Base Plate'.

Figure 39. Cross section of the side view showing the Hard Stop between the 'Mounting Pivot Bracket' and the 'Pivot Pin—Mounting Bracket'.

The 'Vee' and 'Flat' mirror adjustments are identical except for the base; one has a 'V' shape and the other has a flat shape. The adjuster onto the 'Vee' or 'Flat' bases is the 'Adjustment Screw' assembly. A cross section is provided in figure 37. This consists of a long screw with a ball fitted (i.e., the adjustment screw assembly). The material of the alignment ball is specified as high hardness tool steel (UHB Arne 59 HRC).

The alignment ball makes contact with 'Vee' or 'Flat' bases which are attached to the 'Location Bush' and a M30 nut and washer. Pre-loaded contact between the components on the 'Mounting Plate' and the components on the 'Floating Ring Insert' via the alignment balls is ensured by two springs, one on each side of the 'Adjustment Screw' assembly and fitted in tension (see figure 37).

The 'Cone', on the other side, does not have an adjustment screw as an actuator and acts a kinematic constraint (see figures 31 and 38). It is located on top of the 'Baseplate' (see figure 32). The central element is the 'Pivot Pin' (see right hand side of figure 33). The ball end of the 'Pivot Pin' engages in a conical cup in the 'Mounting Pivot Bracket' (see right hand side of figure 34) that is attached to the 'Floating Ring Insert'. Two large bolts (labelled as 'long bolts' in the right hand side of figure 34) go through the 'Mounting Pivot Bracket' as well as the whole thickness of the 'Floating Ring Insert' and the 'Pivot Bracket Closer' thus clamping the 'Floating Ring Insert' to the 'Mounting Pivot Bracket' and the 'Pivot Bracket Closer' (see figure 34). Figure 38 produces a cross section of the front view of the 'Cone' as a kinematic constraint. The new elements to note here are the two springs side by side to the 'Pivot Pin' which are held under tension by the 'Spring Retainer Rod'. The 'Pivot Pin' is fitted into the 'Pivot Pin-Mounting Bracket' which is attached to the 'Base Plate' and the 'Mounting Pivot Bracket' is coupled to it from above.

The 'Cone' set up (see figure 31) enables the 'Floating Ring' assembly to pivot within a small range on the spherical surface of the 'Pivot Pin' and it constitutes the third kinematic contact point (see figure 35).
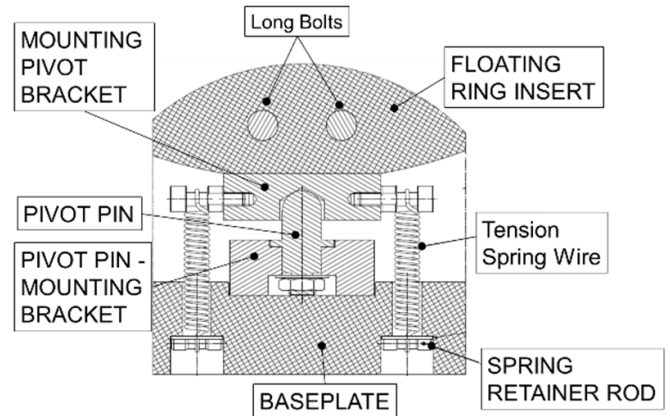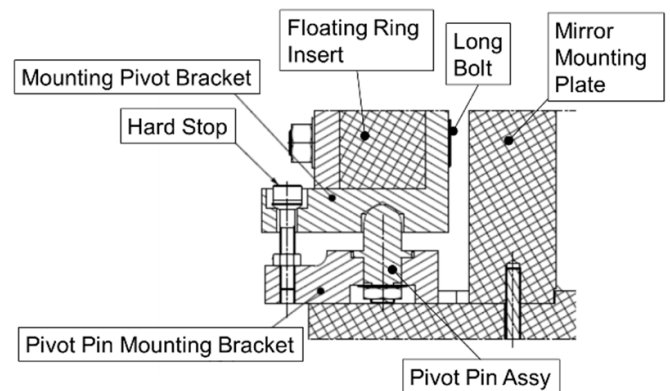
A secondary constraint between the 'Mounting Pivot Bracket' and the 'Pivot Pin—Mounting Bracket' is implemented using a 'Hard Stop' which is simply another bolt of M12 size which is secured once alignment adjustments have been completed (see figure 39).

Finally, an additional two 'Hard Stops' connect the vertical 'M3 Mirror Mounting Plate' with the 'Floating Ring' assembly ensuring both that contact is always maintained at the 'Vee' and 'Flat' and that there is a limited range of travel once aligned adjustments have been made (see figure 40).

6.2.3. Engineering analysis of DIR-M3. The engineering analysis for the DIR-M3 assembly focusses on the 'Mounting Arm' assembly and the hinge assembly (see [25]). The static structural calculations for the 'Mounting Arm' assembly yielded a maximum stress of 86 MPa, which was localised, and a maximum deformation of 1 mm (see [30]). Using the worst-case arm force and moment reactions, the RFs for the welds, bolts and pins were larger than 2 and therefore acceptable. Eddy current loops formed by the three mounting arms were also considered (see [22, 23]), but the disruption loads were
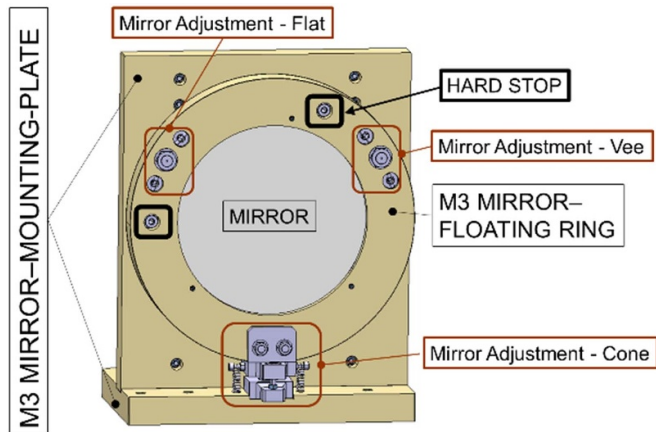
Figure 40. Two 'Hard Stops' for the 'Vee' and 'Flat' adjustments connecting the vertical 'M3 Mirror Mounting Plate' with the 'Floating Ring' assembly.
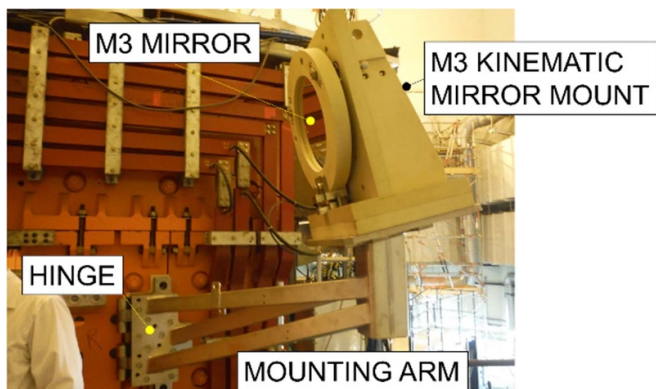

Figure 41. Side view of DIR-M3 after being installed with the hinge in the closed position.

Figure 42. Rear view of the DIR-M3 after being installed with the hinge in the open position.

Figure 43. Photo taken from above of two operatives located on a MEWP closing the hinge and placing the DIR-M3 in the 'closed' position.

found to be small due to the material choice of stainless steel and it was not necessary to introduce insulating breaks in the loops. The ERFA harmonic analysis was performed with both the mirror mounting assembly and the mirror itself as a single point mass for simplicity. The maximum amplitude on the mounting plate considering dynamic amplification is found at a frequency of 7.2 Hz. This peak amplitude corresponds to a mirror rotation of $0.006°$ which is less than required by Zemax tolerancing (see [30]). Regarding the mirror mounting, an analysis of the springs used for the mirror adjustments and the 'Pivot Pin' was also performed to assess the risk of insufficient mirror restraint, since the mirror mount is positioned tilted forward at an angle of $12.90°$ and they were found to be suitable (see [25]). Note that the hard stops provided additional assurance.

6.2.4. Installation of DIR-M3 assembly.   Photos showing the system just after being installed are given below in figures 41 and 42.

Each of the sub-assemblies were put together separately in the labs outside the Torus Hall. The first step of the installation phase was to drill and tap the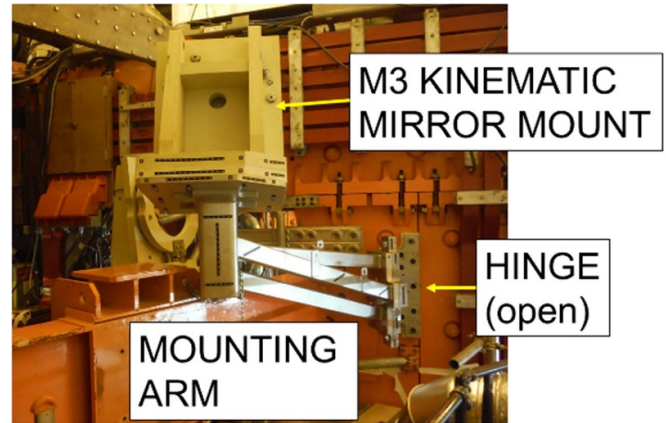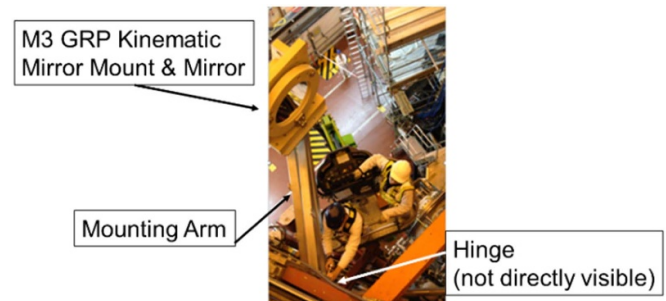 holes in the transformer limb for fixing the interfacing plate. The installation of the 'Mounting Arm' assembly followed, and finally the installation was completed with the mirror mount sub-assembly. A photo taken after DIR-M3 had been installed showing the hinge in the open position is given in figure 42.

Figure 43 shows two operatives on top of a MEWP adjusting the position of the hinge from open to closed.

6.3. DIR M4 assembly

The DIR-M4 assembly is located opposite on the machine to DIR-M3 but such that it can direct the light path towards the DIR penetration on the west wall of the Torus Hall (see figures 18 and 19). Figure 44 shows a side and rear view of the DIR-M4 assembly. In addition, the figure also lists the main sub-assemblies. The total height of the whole assembly is ∼1.1 m.

This section will be subdivided into three subsections, each describing the sub-assemblies listed below:

- Mirror Mounting Frame assembly.
- Mirror Support Plate assembly.
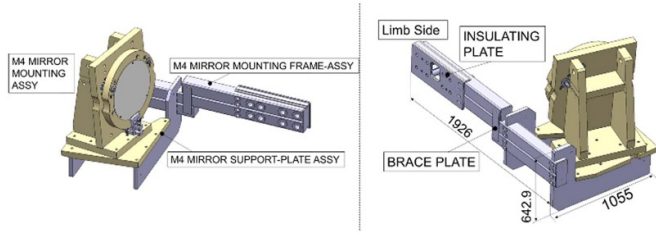- Mirror Mounting assembly.

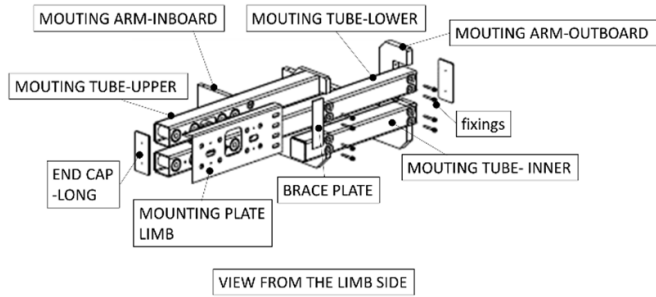**Figure 44.** Side and rear views of the DIR M4 assembly.

Figure 45. Exploded view of the DIR-M4 mirror mounting frame assembly listing the key components.

6.3.1. DIR M4 mirror mounting frame assembly. The 'Mirror Mounting Frame' assembly is attached along the side 5/6 of the transformer limb in octant 5 at a similar height as the DIR-M3 assembly. The total weight of this sub-assembly is 290 kg. There is an electrically 'Insulating Plate' located between the limb face and the mounting frame assembly, which is made from EPM203 (see [21]).

An exploded view of the main components is given in figure 45.

There are three mounting hollowed tubes denoted as 'Mounting Tube—Lower', 'Mounting Tube—Upper' and 'Mounting Tube—Inner' which are made of 316L stainless steel with different lengths and are enclosed with an End Cap' (see figure 45). Bushes are used to ensure that fasteners can be tightened against the walls of the box section mounting tubes without distorting them.

The 'Brace Plate' (see figure 45) is welded to the three mounting tubes in order to provide additional stiffness.

There are two mounting arms (see figures 45 and 46) that serve as a pivot base for the mirror mounting. These two mounting arms are named as 'Mounting Arm-Inboard' and 'Mounting Arm-Outboard'. They both have a similar outline.

The key dimensions (in millimetres) of the two mounting arms are shown in figure 46. The material is 316L stainless steel. The holes on the face of the plates are used for temporary attachment of the lifting frame during installation.

6.3.2. DIR M4 mirror support plate assembly. The 'M4 Mirror Support Plate' (see figure 44) is an interface component to attach the 'Mirror Mounting' assembly to the 'Mirror Mounting Frame' assembly. Figure 47 shows the shape and overall dimensions: 810 mm $\times$ 740 mm $\times$ 62.24 mm. The weight is 52.5 kg. A main feature of this component are the
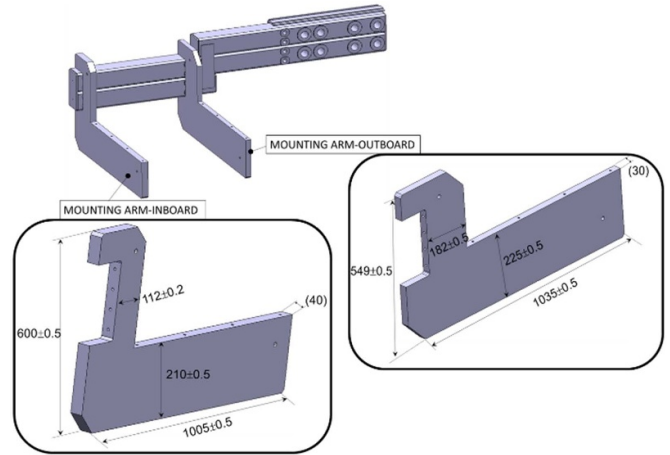

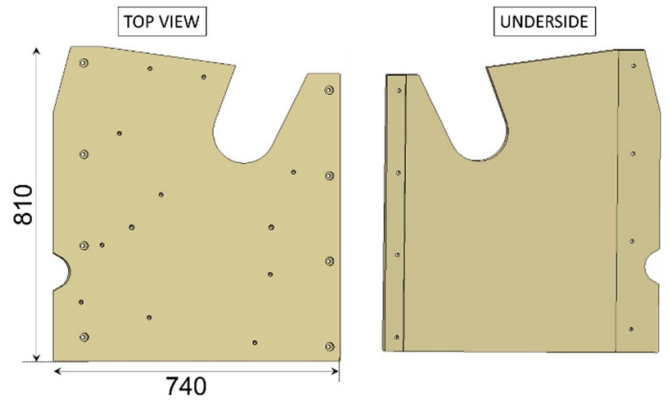**Figure 46.** Model and dimensions (mm) of the mounting arms.

Figure 47. Top and underside views of 'M4 Mirror Support Plate' assembly with key dimensions in millimetres.

cut outs in two of the sides. The largest U-shape cut out is to accommodate the error field correction coil support strut.

6.3.3. DIR-M4 mirror mounting. The mirror mount (see figure 48) is almost identical to the one for DIR-M3. The weight is 246.9 kg. Therefore, this section will only point out the key differences and refer to section 6.2.2 for the detailed description of the components.

The main differences are the cut-outs at both sides of two components: the 'Floating Ring' assembly and the 'Mounting Plate' assembly. The reason for the cut outs on the right-hand side of the front view of figure 48 on both the 'Floating Ring' and the 'Mounting Plate' assemblies is to avoid clashing with the water pipe attached to the transformer limb side at that location. On the other hand, the reason for the cut outs on the left-hand side of the front view of figure 48 is to avoid clashing with the line of sight between the mirrors M2 and M3.

6.3.4. Engineering analysis of DIR-M4. The engineering analysis is divided into the calculations for the mirror mount and the mount support frame (see [22, 30]). Since the mirror mount is identical to DIR-M3 with the exception of the cut
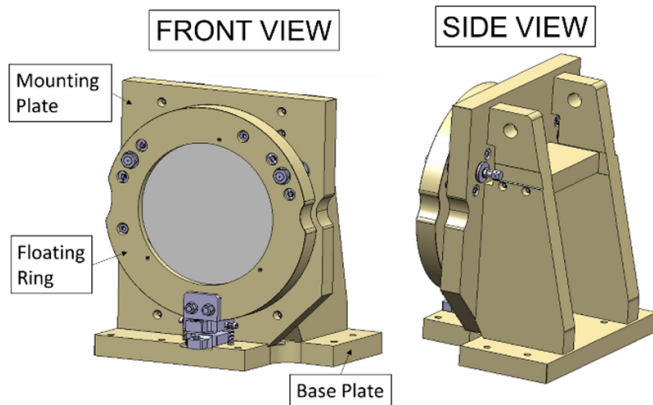
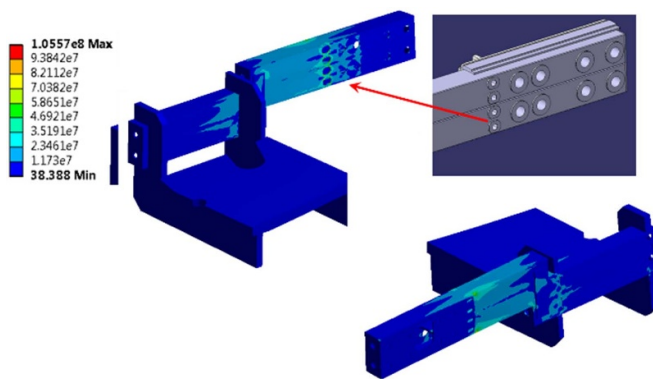**Figure 48.** Front and side views of DIR-M4 mirror mounting.

Figure 49. Model showing static structural stress levels in MPa as a function of colour.

Figure 50. Photo taken after the installation of only the 'M4 mirror mounting frame'.
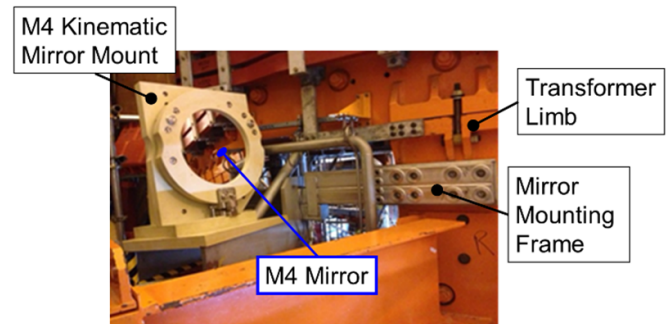
Figure 51. Photo taken after the installation of the DIR-M4 complete assembly.

outs, which do not significantly affect the analysis (as confirmed by investigation), the results reported in section 6.2.3 specifically for the mirror mount are applicable here as well. However, for the 'M4 Mirror Mounting Frame' assembly and 'M4 Mirror Support Plate' assembly, a summary of the results will be presented here.

Starting with the static structural analysis of these two subassemblies, the self-weight equivalent stress levels are depicted as a function of colour in figure 49. The peak value found is 106 MPa but it is considered acceptable because it is constraint related and still below the maximum allowable value of 147 MPa.

The maximum deformation due to self-weight stresses was found to have a peak value of 2.4 mm. This result in itself does not represent a problem as long as it is taken into account during alignment, since this deformation is static and therefore permanent. Furthermore, the RFs for the welds joining the box sections together were larger than 6 and therefore acceptable. Calculations performed for the studs attaching the mounting tubes to the transformer limb included a check that neither gapping nor slip of the studs would occur, which is particularly important for fasteners that pass through 'thick' components ahead of the joint interface.

Secondly, the dynamic deformations corresponding to ERFA kicks were also analysed and found to be allowable.
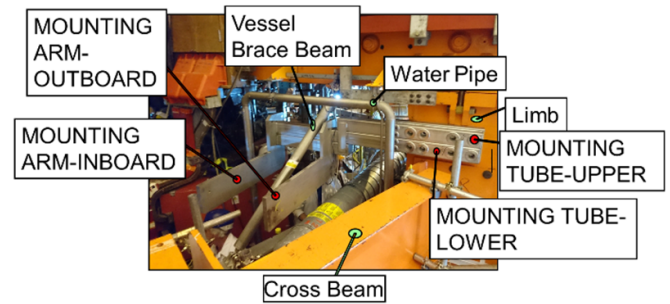
The worst-case value corresponded to a frequency of 40 Hz, and translated into $\pm 0.0008°$ platform rotation, which is considered negligible (see [22]).

6.3.5. Installation of DIR-M4. Before the installation work started, it was necessary to remove a water pipe and a vessel brace beam. In addition, the drilling of the holes and fitting of the limb studs was done after a survey was carried out to position the holes. The lifting was performed with a bespoke lifting frame featuring a novel counterweight arrangement to modify the position of the assembly centre of gravity. The photo in figure 50 describes the first phase of the installation completed with the mounting frame screwed to the transformer limb as well as both the water pipe and the vessel brace beam being re-installed.

Figure 51 shows a photo of DIR-M4 after the entire installation was completed.

7. Penetration and radiation through the biological shield wall

Since the paper dedicated to the WAV LOS includes a detailed description of the function of both WAV and DIR penetrations, including the key components (see [6]), only those elements of the DIR penetration which are different from WAV will be described here. The DIR penetration is shorter than the WAV penetration with a length of 3318 mm. In addition, the DIR penetration is positioned at an angle with respect to the WAV one. The specific tilt of the penetration tube was a compound
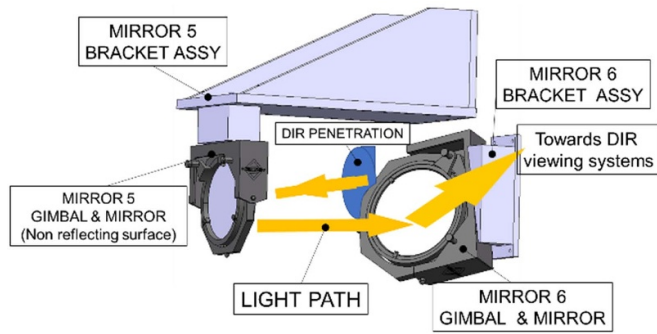
Figure 52. DIR M5 and DIR M6 mirror assemblies located outside the Torus Hall. The outside of the biological shield wall is not shown. The yellow arrows represent the light path. The DIR penetration is shown as a dark blue circle opposite M5.

angle defined by the optical modelling. Secondly, regarding radiation levels in the lab outside the biological shield, a neutronics analysis and description of the neutron shielding has also been explained in detail in the paper dedicated to the WAV LOS (see [6]).

8. Mechanical design of mirror assemblies outside the Torus Hall

The design of the mirror mounting outside the biological shield wall is simpler in terms of the selection of materials because of factors such as radiation and electromagnetic forces no longer playing a role.

There are two mirror assemblies located outside the Torus Hall which are referred to as DIR-M5 and DIR-M6 (see figure 52). The mirror assemblies are located in one of the new labs constructed outside the Torus Hall for this purpose which is known as the 'Middle Lab'. This lab, as explained in [6], was built on the outside of the biological shield wall and it also houses the DIR penetration. The material used for all the metal brackets is Aluminium alloy.

The overall dimensions for the M5 complete bracketry are: 900 mm × 400 mm × 468.2 mm. The mounting assembly consists of a number of plates and one block which the M5 gimbal mirror mount is attached to (see figure 52).

The overall footprint dimensions for M6 supports are: 400 mm × 160 mm × 145 mm. M6 uses an angled block to which the gimbal mirror mount is fixed to.

In both cases, the brackets were fixed to the outside of the biological shield wall using HILTI (www.hilti.co.uk/) resin-bonded anchors. The data sheet for the gimbal mirror mounts is provided in [31].

9. Mounting of DIR cameras outside the Torus Hall

The cameras were mounted in the same lab as the one for the penetration, denoted as 'Middle Lab'. A schematic is provided in figure 53. The penetration is not visible in figure 53 as from
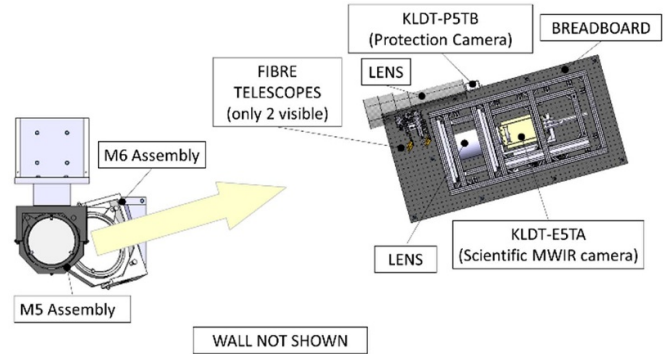

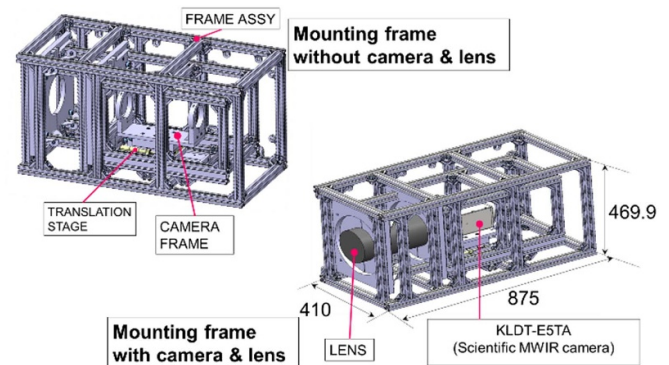**Figure 53.** Schematic of the DIR assemblies in the 'Middle Lab'.

Figure 54. Mounting frame for KLDT-E5TA.

this view it is located behind M5. The yellow arrow represents the light path from M6 towards the viewing systems mounted onto the optical breadboard. Furthermore, the optical breadboard is then attached to the outside of the biological shield wall using HILTI resin-bonded anchors.

This section will focus on the mounting frame used for the scientific MWIR camera (KLDT-E5TA) given on figure 54. The overall dimensions are: 875 mm × 410 mm × 469.9 mm. The mounting frame forms a cage around the optics and camera device. However, there are two mounting frames, one inside the other. The outer one that holds the lens and the inner one that holds the camera to the lens (see figure 54). This mount enables the alignment of the whole lens and camera combination with respect to the light path and field of view as well as the alignment of the camera to the lens (i.e., focus and field of view to match the detector in translation and rotation). The lens is secured by a set of clamping plates (see figure 54).

It uses the same concept as the one described in the WAV paper (see [6]). The embedded inner frame also incorporates a translation stage to enable moving the camera precisely along its optical axis with respect to the lens (see figure 54). In addition, it includes a stop to lock the camera into position once the focusing is complete. A photo of the front view of all the DIR viewing systems inside the 'Middle Lab' is shown in figure 55.
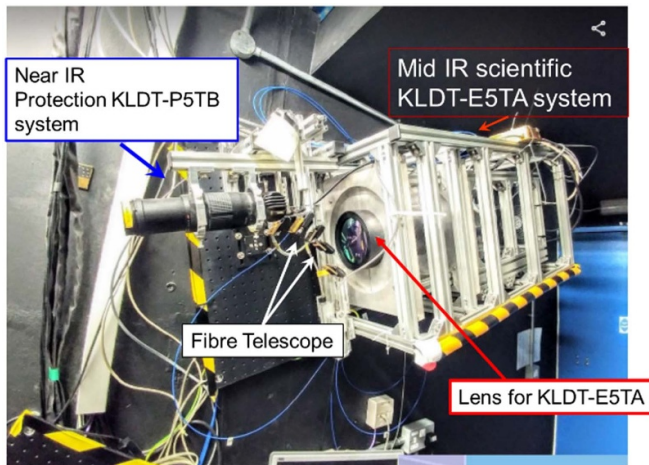
Figure 55. Photo showing DIR viewing systems inside 'Middle Lab'.

10. Operational experience

The design and construction of an optical relay diagnostic line of sight which covers 31 m presents a significant engineering challenge of preserving image stability in the presence of high and rapidly changing magnetic fields. This key performance requirement was discussed for the WAV line of sight (see [6]) and it is reported here for the DIR line of sight.

A review of the performance of the system once it was installed and operational but prior to the D-T campaign, was carried out, and it was found that the achieved image stability was not fulfilling the operational requirements (see [32]) which can be summarised as being to produce images on the protection camera reproducible/stable at the level of 1 pixel. The performance review showed that the highest amplitudes found in a few pulses corresponded to ~10 pixels peak to peak in the toroidal image direction and 17 pixels peak to peak in the radial image direction (see [33]). The pixel size (15 μm) is the same for the protection camera (KLDT-P5TB) and the scientific camera (KLDT-E5TA). The associated frequencies for the highest amplitude were in the range 225–241 Hz which is aligned with the predicted mode 3 frequency obtained from the harmonic analysis (see figure 25). The larger than expected vibration amplitude may occur because, although the geometry was designed to minimise the out-of-phase movement between mirrors M1 and M2 for the primarily in-phase mode 3, relatively small inaccuracies in the model representation of reality could have a relatively large effect on the cancellation of the out-of-phase component. The root cause for the image instability was identified to be due to deflections of the order of tens of microns of the M1 and M2 mirrors (see sections 6.1.3 and 6.1.4) caused by eddy current loads on the metallic mirror mounts. During the design phase, the decision of selecting COTS metallic mirror mounts for the relatively small mirrors M1 and M2 was considered a lower risk in comparison with designing non-metallic kinematic mirror mounts in house. This made the minimisation of differential rotation between mirrors M1 and M2 more challenging than if a custom mount had been designed to hold both M1 and M2.

The risk was assessed oppositely for the large mirrors since the commercial option was neither realistic nor forthcoming and the predicted impact of the magnetic fields for the performance of the large mirrors in the optical relay, if they were to be metallic, was highly significant. The possibility of redesigning the mounting for mirrors M1 and M2 after operational experience was not possible because altering the current system would automatically invalidate the present (absolute) calibration of the cameras. Secondly, the possibility of retrofitting additional components (as was undertaken for the WAV LOS to improve the image stability, see [6]) was not possible because of the difficulty in accessing all sides of the L1-M1-M2 mirror assembly together with the risk of misaligning the system, which again would invalidate the calibration. Nevertheless, it was found that it was possible to fulfil the required functionality of the camera systems (see [32]) via different routes which will be explained below.

Starting with the protection camera (KLDT-P5TB), this system is capable of measuring surface temperatures of specific areas within the field of view. These areas, known as 'ROIs', have measured temperature contour maps created for them covering different tiles within the field of view. As shown in figure 4, the field of view for KLDT-P5TB comprises Tile 5, Tile 6 and Tile 6 extension mainly. In order to mitigate the effect of the image movement, the use of ROIs suitably larger than the image movement's amplitude has proven sufficient as a mitigating technique—the feature/position of main interest is always within the ROI despite the image movement. This has been applied to Tile 5 and Tile 6. For Tile 6 extension, however, this approach was not possible for both radial and toroidal axes because the visible Tile 6 extension width toroidally is only ~10 pixels. In addition, the surface of the Tile 6 extension had already begun to show some signs of coating degradation which produced localised 'hot spots'. These 'hot spots' appear to be measurements of very high surface temperature measurements of the tile with a characteristic fast temperature increase relative to slower and lower surrounding area surface heating under sustained thermal load. However, they are as a result of local modifications to the tile surface, not the result of actual bulk heating of the tile. Since these hot spots are not static, the best way to mitigate their effects is the combination of complimentary camera systems. During the D-T campaign, this was realised using the protection cameras for WAV LOS and DIR LOS.

The impact on the scientific mid-infrared camera (KLDT-E5TA) was mitigated by the use of a software to correct for the image movement after the video has been recorded. This has also proven to be successful in delivering accurate surface temperatures and heat fluxes post pulse. This approach, however, was not possible to apply it onto the protection system due to relatively slow operational frame rate (30 Hz) of the protection cameras in comparison with the scientific camera (>2 kHz).

Information regarding the calibration of the cameras has already been accounted for in the paper dedicated to the WAV LOS (see [6]) and it will not be mentioned again here.

As mentioned in section 3, three labs were constructed in the vertical direction in the building adjacent to the outside of

the biological shield wall. These labs were named as 'Upper Lab', 'Middle Lab' and 'Lower Lab' and their function is the housing of all the camera systems. The 'Upper Lab' is used only for the auxiliary equipment such as PCs, network devices and power supplies whereas the 'Middle Lab' and the 'Lower Lab' are used to house all the camera systems. However, the camera systems which form part of the DIR LOS were all installed in the 'Middle Lab'. It is only the WAV LOS (see [6]) which uses the 'Middle Lab' and 'Lower Lab' for the camera systems associated to this line of sight.

Access to all three labs was possible during the D-T campaign, when the tokamak had controls in place which prevented it from pulsing. This was still very advantageous because access to the Torus Hall during the D-T campaign was not permitted due to the high level radiation dose. This dose was produced by the 14 MeV D-T neutron yields which were higher than 10^{18} neutrons. Furthermore, during the subsequent Deuterium campaigns, the 'Upper Lab' was accessible at any time (i.e., even during a pulse).

A final note to add is regarding the reliability. The reliability of the DIR LOS has proven to be very successful with regards to the optical alignment and mechanical stability of the GRP kinematic mirror mounts (DIR-M3 and DIR-M4) and the camera performance in general. Furthermore, in terms of operational time lost, only two faults were reported during the D-T campaign specifically related to the DIR line of sight. These two faults were due to communication issues between the PC and the KLDT-P5TB camera and they were network related. These two faults took less than 10 min each to be resolved. Finally, an important factor from the operational experience aspect is the control of the temperature and humidity in the 'Middle Lab'.

11. Conclusions

The opto-mechanical design and installation for a remote optical relay line of sight to view the divertor tiles from outside the Torus Hall in JET has been presented in this article. This remote line of sight includes a number of viewing systems which are not affected by the high neutron flux from the experiments during the D-T campaign since the viewing systems are located outside the biological shield wall. The viewing systems operate in the near and middle infrared wavelength range. This line of sight comprises an optical mirror relay which includes two novel large GRP kinematic mirror mounts standing vertically. Operational experience has shown that the performance of GRP kinematic mirror mounts has been very successful. In particular, they avoid the vibration issues that were found to occur in some locations where conventional electrically conducting mirror mounts were used and experienced induced eddy currents from the fusion environment. Finite element harmonic analysis was reasonably successful in substantiating the design with regard to vibration induced image movement but, with hindsight, it would have been prudent to demand higher RFs to allow for modelling uncertainties. The optical modelling and camera performance have met also successfully the project requirements. A separate paper to cover

a second line of sight which produces a wide-angle view is recommended to the reader since there are parts of the description of this line of sight which have been explained further in the paper related to the wide angle view line of sight. The results and operational experience reported in this paper can also be of interest for similar diagnostics requirements at ITER.

Data availability statement

All data that support the findings of this study are included within the article (and any supplementary files).

Acknowledgments

ORCID iDs

I Balboa https://orcid.org/0000-0002-5665-2222
S A Silburn https://orcid.org/0000-0002-3111-5113
A Huber https://orcid.org/0000-0002-3558-8129
C Perez Von Thun https://orcid.org/0000-0002-1166-2179
J Karhunen https://orcid.org/0000-0001-5443-518X

References

[1] JET press conference Deuterium-tritium experiments set new fusion energy record (available at: https://youtu.be/ibMG5iUtF6w)
[2] Maillux J *et al* 2022 *Nucl. Fusion* **62** 042026
[3] Belonohy E *et al* 2017 *Fusion Eng. Des.* **123** 196–200
[4] Figueiredo J *et al* 2016 *Rev. Sci. Instrum.* **87** 11D443
[5] Figueiredo J *et al* 2018 *Rev. Sci. Instrum.* **89** 10K119
[6] Balboa I *et al* 2023 *Plasma Phys. Control. Fusion* **65** 064005
[7] Huber A *et al* 2018 *Nucl. Fusion* **58** 106021
[8] Silburn S A *et al* 2017 *Phys. Scr.* **T170** 014040
[9] Paméla J, Matthews G F, Philipps V and Kamendje R 2007 *Nucl. Mater.* **363–365** 1–11
[10] Hobirk J *et al* 2012 *Plasma Phys. Control. Fusion* **54** 095001
[11] Garzotti L *et al* 2019 *Nucl. Fusion* **59** 076037
[12] Matthews Guy *et al* 2013 *Nucl. Mater.* **438** S2-S10
[13] Joint European Torus (Available at: https://en.wikipedia.org/wiki/Joint_European_Torus)
[14] Sieglin B, Faitsch M, Herrmann A, Brucker B, Eich T, Kammerloher L and Martinov S 2015 *Rev. Sci. Instrum.* **86** 113502

[15] Huber V *et al* 2017 *Fusion Eng. Des.* **123** 979–85
[16] IGAR 12-LO Pyrometer datasheet (available at: www.
advancedenergy.com/products/temperature-measurement/
thermal-measurement-optical-pyrometers-power-
controllers/metal-applications-pyrometers/impac-isr-12-lo-
igar-12-lo/)
[17] Stamp M F 2015 Technical report no.
UKAEA-CCFE-RE(23)14 (UKAEA Culham Science
Centre)
[18] Stamp M F 2015 Technical report no.
UKAEA-CCFE-RE(23)15 (UKAEA Culham Science
Centre)
[19] (Available at: www.canon.co.uk/lenses/ef-75-300mm-f-4-5-6-
iii-lens/)
[20] Silburn S A 2015 Technical report no.
UKAEA-CCFE-RE(23)16 (UKAEA Culham Science
Centre)
[21] Durostone® EPM203 (available at: www.roechling.com/uk/
industrial/materials/composites/epoxy-resin/durostone-
epm-203)
[22] Williams J C *et al* 2015 Technical report no.
UKAEA-CCFE-RE(23)17 (UKAEA Culham Science
Centre)
[23] Williams J C Technical report no. UKAEA-CCFE-RE(23)18
(UKAEA Culham Science Centre)
[24] E De la Luna *et al* 2016 *Nucl. Fusion* **56** 026001
[25] Williams J C Technical report no. UKAEA-CCFE-RE(23)19
(UKAEA Culham Science Centre)
[26] Williams J C Technical report no. UKAEA-CCFE-RE(23)20
(UKAEA Culham Science Centre)
[27] Stamp M F Technical report no. UKAEA-CCFE-RE(23)21
(UKAEA Culham Science Centre)
[28] Haist B, Mills S and Loving A 2009 *Fusion Eng. Des.*
84 875–9
[29] ING Cryostat alignment and focusing (available at: www.ing.
iac.es/astronomy/instruments/isis/alignment.html)
[30] Williams J C *et al* Technical report no.
UKAEA-CCFE-RE(23)22 (UKAEA Culham Science
Centre)
[31] A0M110 aerotech mounts (available at: www.coherent.com.
au/products/motion-control/optical-mounts/aerotech-aom-
optical-mount-1286.html)
[32] Fishpool G Technical report no. UKAEA-CCFE-RE(23)25
(UKAEA Culham Science Centre)
[33] Silburn S A Technical report no. UKAEA-CCFE-RE(23)26
(UKAEA Culham Science Centre)